UiT
THE ARCTIC UNIVERSITY OF NORWAY

Faculty of Science and Technology

Department of Physics and Technology

Maritime Target Detection in Non-homogeneous Sea Clutter Environments based on Single- and Multi-polarization Synthetic Aperture Radar Data

—

Ding Tao

A dissertation for the degree of Philosophiae Doctor – September 2015

UNIVERSITY OF TROMSØ

Abstract

This thesis discusses the subject of maritime target detection based on single- and multi-polarization synthetic aperture radar (SAR) data. The primary objective is to develop an automatic and effective target detection algorithm, which is able to provide robust performance for an operational maritime surveillance system under various circumstances.

The conventional constant false alarm rate (CFAR) detector setup is adopted in the algorithm, which relies on accurate statistical characterization of the background sea clutter measurements. The local reference clutter is confined using a modified sliding window technique. Note that there are two major detection issues that are frequently encountered and have been identified in many previous studies. Firstly, in multiple-target situations, the local reference sea clutter is often contaminated by interfering targets. The outcome is known as the *capture effect*. Secondly, in non-homogeneous environments, sea surface transitions between regions with different radar backscattering properties are usually observed in conjunction with various meteorological and oceanographic phenomena. The result is recognized as the *clutter edge effect*. Both effects inevitably lead to inaccurate parameter estimation and deceptive statistical modeling, thus causing severe degradation of the CFAR detection performance.

To understand the statistics of sea clutter in multi-polarization SAR data, it is natural to study the covariance matrix derived from the scattering vector, since it holds all polarimetric information and its estimate is an important factor for many statistical models. Despite the attempts of modeling the real sea clutter with more comprehensive models, mixed and/or contaminated clutter is always difficult to handle, which is demonstrated in this thesis using a test with log-cumulants. Therefore, truncated statistics (TS) is first reviewed as a useful tool for analyzing the region of interest (ROI) contaminated by multiple non-clutter pixels. Unlike a similar data censoring approach, the rigorous statistical analysis using TS provides improved background clutter modeling results, and does not require prior knowledge of the interfering pixels. A corresponding TS-based CFAR (TS-CFAR) detector is then designed to suppress the capture effect and ameliorate detection performance. Furthermore, building upon the idea of predetermining the class information within the ROI, an automatic image segmentation stage with suitable statistics is adopted in the detection scheme to address the clutter edge issue. After the data truncation, which excludes potential interfering pixels, a finite mixture modeling using TS is performed with a modified expectation maximization (EM) algorithm. The obtained statistical information of the local reference clutter is then passed to the final pixel-wise CFAR detection stage.

The end product is a segmentation based CFAR detection algorithm using TS. Single-look intensity (SLI) and multi-look intensity (MLI) SAR imagery are mainly targeted in this study for directly supporting operational applications, where intensity measurements based on single- or dual-polarization data are mostly applied. Instead of the conventional product models, the sea clutter samples are modeled based upon a mixture of the truncated two-parameter gamma models. It has been demonstrated on several real SAR images, that the proposed algorithm is able to adapt to various contaminated

non-homogeneous environments, provide improved local background clutter modeling, and deliver robust detection performance.

Acknowledgements

Foremost, I would like to express my sincerest gratitude to my main supervisor, Camilla Brekke, for years of patience and motivation, for the continuous support of my Ph.D study and related research. She truly puts herself for the sake of students, and I could not have imagined having a better supervisor for my Ph.D study. Next, I would like to thank my co-supervisors and co-authors, Stian N. Anfinsen and Anthony P. Doulgeris for being my mentors and friends in all the time, for their extraordinary guidance and help through all stages of research, and for every discussions and hard questions which encouraged me to expand my research from various perspectives. My thanks also go to Torbjørn Eltoft, Harald Johnsen and Yngvar Larsen for their insightful comments and immense knowledge. I look forward to continuing these wonderful friendships and can not wait for more great collaborations in the future.

Moreover, my sincere thanks go to UiT – The Arctic University of Norway and the Department of Physics and Technology for the study opportunity and the first-class scientific research environment. Meanwhile, the Ph.D work would have been impossible without the funding from the Norwegian Research Council through the ArcticEO project and the precious data and information support from Norut Northern Research Institute, Kongsberg Satellite Services (KSAT), Kongsberg Spacetec, and the Norwegian Meteorological Institute. Special thanks to Dr. Armando Marino at ETH Zürich, Institute of Environmental Engineering for sharing valuable RADARSAT-2 SAR datasets from Portsmouth, UK. In addition, my warmest thanks to Marit K. Hall and Evelyn H. Mohus from the department and university administration for helping me get through my work-related and personal life in Tromsø.

Furthermore, deepest thanks to Thomas Kræmer for being an excellent office mate, for sharing his knowledge and ideas during countless academic discussions, for his selfless helps in all aspects, and most importantly for being my best friend. I wish I could have another four years to work with you and learn from you. My heartfelt thanks also go to all the members in our group, Jakob Grahn, Mari-Ann Moen, Stine Skrunes, Ane S. Fors, Vahid Akbari, Temesgen Yitayew, etc. Thank you for making it such a great place to work, and for giving me so many precious memories, like the amazing road trip to Nordkapp with Thomas and Jakob, the Christmas party at Mari-Ann's house every four years, the SPIE conference at Edinburgh with Stine, all the exciting hiking and skiing trips, and the numerous homemade cakes for every occasion. No enough words can fully express my feelings. You are the best!

Finally, I would like to express my love and gratitude to my family, because I could never have done this without you. I thank my parents for their unlimited supports through my whole life, my wife Xiaojin Qiu for her encouragement, comfort, and patience in all those years, and my girl Jinxuan for becoming the best part of my life.

I dedicate this thesis to you all.

Contents

List of Acronyms

2D	Two-Dimensional
AIS	Automatic Identification System
AP	Alternating Polarization
ArcticEO	Arctic Earth Observation and Surveillance Technologies
ASI	Italian Space Agency
CA	Cell Averaging
CCRS	Canada Centre for Remote Sensing
CCT	Centre Canadien de Télédétection
CDF	Cumulative Distribution Function
CFAR	Constant False Alarm Rate
COSMO-SkyMed	COnstellation of small Satellites for the Mediterranean basin Observation
CUT	Cell Under Test
dB	Decibel
DLR	German Aerospace Center
EM	Expectation Maximization
EMSA	European Maritime Safety Agency
ENL	Equivalent Number of Looks
ESA	European Space Agency
FFI	Norwegian Defense Research Establishment
GEC	Global Environmental Changes
G-ML	Gaussian distribution based Maximum Likelihood
GO	Greatest-Of
GPS	Global Positioning System
HF	High Frequency
HH	Horizontal transmit, Horizontal receive polarization
HV	Horizontal transmit, Vertical receive polarization
Hz	Hertz
EO	Earth Observation
IC	Iterative Censoring
IEA	International Energy Agency
IMO	International Maritime Organization

IPCC	Intergovernmental Panel on Climate Change
ISR	Internet Ships Registry
K-ML	$\mathcal{K}$ distribution based Maximum Likelihood
KSAT	Kongsberg Satellite Services
MDA	MacDonald, Dettwiler and Associates Ltd.
MLC	Multi-Look Complex
MLI	Multi-Look Intensity
NASA	National Aeronautics and Space Administration
NCA	Norwegian Coastal Administration
NOAA	National Oceanic and Atmospheric Administration
NOFO	Norwegian Clean Seas Association for Operating Companies
NSC	Norwegian Space Center
NSIDC	National Snow and Ice Data Center
ODV	Ordered Data Variability
OS	Ordered Statistic
OPEC	Organization of the Petroleum Exporting Countries
PD	Probability of Detection
PDF	Probability Density Function
Pfa	Probability of false alarm
PolSAR	Polarimetric Synthetic Aperture Radar
PRF	Pulse Repetition Frequency
PTM	Pulse Time Modulation
RCS	Radar Cross Section
ROC	Receiver Operating Characteristics
ROI	Region of Interest
RS	remote sensing
SAR	Synthetic Aperture Radar
SIRP	Sustainable Investment Research Platform
SLC	Single-Look Complex
SLI	Single-Look Intensity
SO	Smallest-Of
TCR	Target to Clutter Ratio
TM	Trimmed Mean
TS	Truncated Statistics
UAV	Unmanned Aerial Vehicle
UHF	Ultra High Frequency
UN	United Nations
US	United States
VH	Vertical transmit, Horizontal receive polarization
VHF	Very High Frequency
VI	Variability Index
VV	Vertical transmit, Vertical receive polarization
WWII	World War II

Chapter 1

Introduction

This chapter presents an overview of the thesis. It begins with the motivation and research background. Then, the objectives and scope of the study are introduced, followed by summaries of the four research articles included. A list of other associated published works is included at the end.

The remaining parts of the thesis are organized as follows. Chapter 2 introduces the fundamentals of maritime target detection using synthetic aperture radar (SAR), which include the basic concepts of polarimetric SAR, essential statistical analysis of sea clutter, short introduction of the constant false alarm rate (CFAR) detection algorithm, and brief reviews of the primary target detection issues and different CFAR detection schemes. The four research articles that contain the research contributions of this thesis are included in Chapters 3–6. Finally, Chapter 7 gives the concluding remarks and future perspectives.

1.1 Motivation

Detection of targets, e.g., vessels, icebergs and oil spills, is the key component for many operational maritime surveillance services, where high quality images of the Earth produced by air- and space-borne SAR systems have been used extensively. The obtained output data are essential for corporations and governments to effectively manage the sea in a sustainable way. The aim of this thesis is to contribute in the field of maritime target detection, focusing on vessel detection.

SAR, as an active remote sensing (RS) technique (see chapter 2.1), is capable of providing useful sea surface information in all weather conditions independent of daylight. For the wide maritime human activities, the recent target detection service based on SAR systems has become an invaluable complement to the existing Global Positioning System (GPS) and Automatic Identification System (AIS). Such a service has already been applied in many practical applications, covering maritime navigation, safety monitoring, security concern, and environment observation for both civil and military purposes. There are also a growing number of new advanced SAR systems in the plan, and

will soon be put into use.

In real cases, a robust and effective target detection algorithm based on the emerging SAR products are largely demanded by operations that are responsible for the safety at sea, fisheries protection, national security, etc. For instance, often as the economical drive for many port cities, heavy traffic in the harbor area needs to be carefully guided and monitored at all times. For security concerns, especially along the sea borders, the increasing risks of smuggling, human and drug trafficking, and illegal immigrants are on the rise in recent years. To control the vast sea regions, the field inspectors require a robust automatic system, which can cover large areas all year long. Nowadays, humans are exploring further into the sea for food, energy and other natural resources, particularly into the warming Arctic region. For example, Norway, as one of the many coastal counties, has an ocean area seven times larger than the land area. The requirements for a national capability to manage and monitor its coastal waters and the Barents Sea increase with the booming shipping, fishing, and other offshore industries. Thus the modern space-borne SAR technique presents a promising option for services supporting the operations of the Coast Guard and other authorities. Moreover, hundreds of thousands of fleets connecting the whole world daily definitely bring urgent demands for better navigation services, and with the growing threats of the global environmental changes, the degree of risk due to wild storms, tsunamis or other natural disasters have increased dramatically for the fishing, shipping, and oil and gas industries. Meanwhile, the corresponding environmental instances like oil spills are more and more common, which puts higher requirements on maritime monitoring and forecasts as well.

1.2 Research background

This section provides a brief summary of maritime human activities and discusses the current state of operational satellite-based maritime surveillance services.

1.2.1 Maritime human activities

For centuries, the sea has been a major hub of human activities, ranging from traditional activities like fishing and shipping to more modern instances such as offshore facilities for natural resources. Never before have so many people lived so close to the coasts, and have so many vessels explored further into the vast sea. In fact, over half the world's population lives within 200 kilometers of a seacoast, as for eight of the top ten largest cities, according to the United Nations (UN) Atlas of the Oceans [1]. Without exaggeration, mankind has been deeply relying on the sea for a long time.

Despite the development of cars, trains and airplanes, shipping remains the major means for transporting raw materials, consumer goods, and energy internationally. Nowadays, over 90% of global commerce is carried by approximate $90,000$ marine vessels [2,3], and the market has been expanding steadily with international trade increasing. Although, most major countries agree that the open seas should remain free to

all shipping in peacetimes, the capability of possessing the command of the sea (or sea control) is still the very symbol of global power from military aspects [4]. This dominance not only applies to one nation's surrounding waters, but also extends far into the vast sea. Since the development of radar technology during World War II (WWII), advanced navies and organizations have begun to use it to provide target information and early warnings. In recent years, safety and security concerns along shipping lanes and sea borders are on the continuous rise all over the global. Different all-weather navigation and assistance systems have been developed to minimize the probability of unwanted incidents at sea. While current examples of piracy [5] off the coast of Somalia and in the Indian Ocean, illegal immigrants from Africa to European countries via the Mediterranean Sea, and human and drug trafficking and other smuggling activities elsewhere, still show huge potentials of new radar surveillance systems with improved target detection ability.

Additionally, the exploration and production of the natural resources in the sea have also become the major drivers of economic growth for many nations. Firstly, as an ancient hunting activity, fishing has always been very important and influential to the human society and economy. In recent years, the fishing industry is driven mostly by the endless customer demands and intense competitions between fleets, which means that most fishing vessels often have to go further into the oceans to find new fishing grounds. Secondly, the offshore oil and gas industry has become an important part to the global energy supply, thanks to the technological developments within the past years. Despite the high risk and safety concerns of the offshore projects, the energy resources production has been accounting for almost one third of the world's production and 55% of non-OPEC (Organization of the Petroleum Exporting Countries) reserves since 2012, according to the International Energy Agency (IEA) [6]. However, it is worth noting that the world's seas prosperity has been threatened by the increasing risk of unsustainable developments and illegal practices around the world.

Meanwhile, human activities can have major impacts on the sea environment and sometimes cause severe environmental disasters. Seriously negative events with long-term consequences have become increasingly common, which can result from technical accidents, human or mechanical failures or carelessness. For instance, the recent Deepwater Horizon oil spill in the Gulf of Mexico 2010 (also known as the BP oil spill or Macondo accident) is considered the largest accidental marine oil spill in history, which caused devastating effects to the offshore and coastal environments and the oceanic lives. Also, a large number of small-scale operational discharges from the shipping vessels are responsible for a huge volume of oil released into the sea [7]. Such practices are illegal, but occur frequently all over the world. In Norway, together with the Norwegian Coastal Administration (NCA), the Norwegian Clean Seas Association for Operating Companies (NOFO) was established to prevent and respond to those potential incidents.

In summary, effective countermeasures for those issues have been demanded by global corporations, government administrations, and environmental organizations for years. New diverse surveillance services based on advanced SAR system, satellite-

based AIS, and existing GPS have shown great potential. As the important part of such operations, maritime target detection has been a necessary role in various incidents. A brief review of current operational maritime surveillance services is provided in the next section.

1.2.2 Operational maritime surveillance services

An important maritime surveillance system is the automatic identification system, which was conventionally designed as a VHF (Very High Frequency) communication system providing information of vessels and offshore platforms [8]. Valuable data, such as vessel location, identification, course and speed, can be exchanged via the system, which allows vessels, coastal guards, customs and other authorities to monitor the traffic at sea and response to abnormal incidents within certain jurisdiction [9–13]. The main goals of an AIS system include providing navigation aids, anticipating and avoiding collisions, and helping search and rescue organizations.

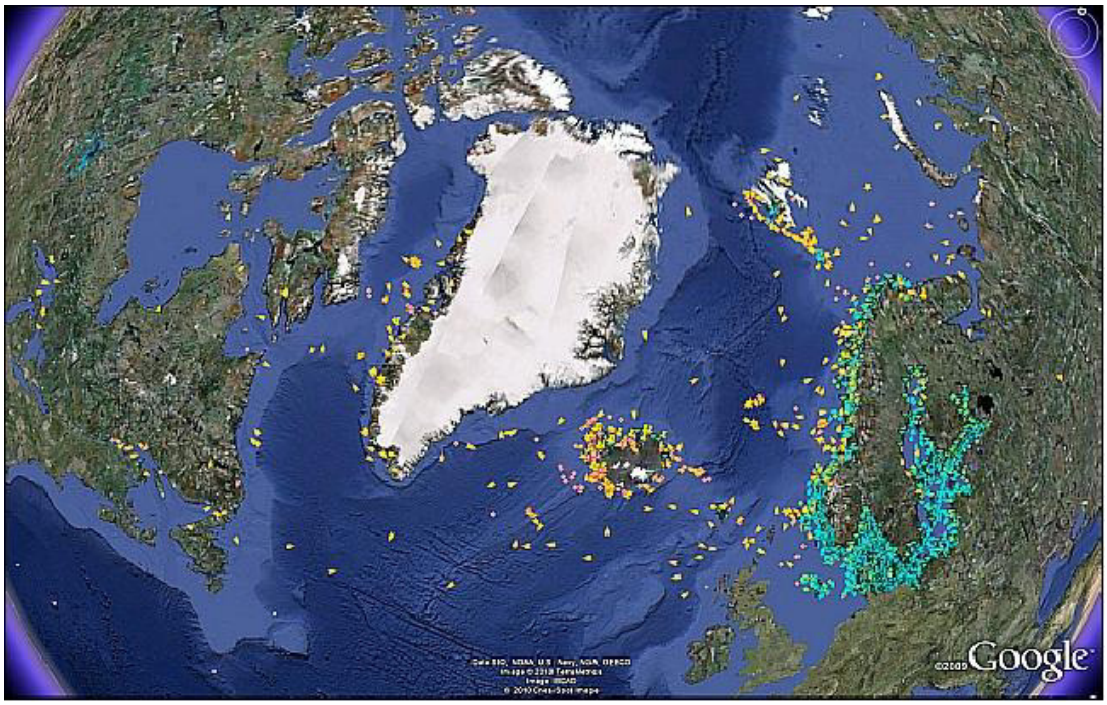

Figure 1.1: The first AIS data from AISSat-1 presented in [9, 10]. The colored symbols mark the AIS data received within the region. Image credit: Google, KSAT, FFI.

Since normal terrestrial AIS system has limited range from coastlines, a satellite-based AIS system has been proposed for its potential coverage of any area on Earth. For instance, AISSat-1 (launched on 12^{th} July 2010) and AISSat-2 (launched on 8^{th} July 2014) are the Norwegian AIS satellites funded by the Norwegian Space Center (NSC) with program management by the Norwegian Defense Research Establishment (FFI)

[9, 10]. They are experimental nano-satellites to receive and forward signals from the vessel's AIS onboard, mainly covering the coastal waters of all oceans Norway manage. The received data have shown large number of vessels outside range of terrestrial AIS networks. Figure 1.1 shows an example of the AISSat-1 reports from the High North on 15^{th} July 2010 [9, 10]. There are a number of currently ongoing trial projects funded by the European Space Agency (ESA) and the European Commission as well [12], such as the RUBIN 7 and 8 AIS missions from LuxSpace/OHB, the COMDEV NTS nano-satellite mission and the US military satellite TacSat-2.

Note that the International Maritime Organization (IMO) requires for most vessels to be equipped with an AIS transceiver, capable of transmitting real-time information to other vessels and to coastal authorities automatically [11, 14, 15]. However, the biggest problem of the system is that people (vessels) can deliberately switch off their transmitter to become invisible to other vessels and the administered surveillance. Therefore, there may be an unusually low number of vessels reported via the system in some regions. For instance, illegal fishing activities have often been difficult to detect and prove in the open sea or near the border of fishing grounds. For busy shipping lanes, pirates can use the AIS reports to spot and attack certain vessels, while the captain of a vessel also has the right to switch off the AIS, either for the safety of the ship or to take other possible routes [9].

Therefore, an active RS system can act as a valuable complement to the existing AIS, and the obtained data can provide additional information for selected areas of interest. Nowadays, many advanced RS systems have been or are about to be put into operation, while space-borne maritime monitoring systems using SAR in particular have shown great application prospects. The advantages of a space-borne SAR include all-weather, 24-hour, large area, frequent and repetitive coverage of an area of interest, and relatively low cost. Operationally, a space-borne SAR target detection system and AIS can be combined for monitoring remote regions, which provides the opportunity to expose vessels that do not send mandatory AIS reports. Although spatial resolution may be a concern of such space-borne system, many latest SAR sensors are capable of producing imagery with high sub-meter resolution. Currently, there are several SAR missions providing images for research and operational applications, which are also commercially available to most civilian users. For examples, operational missions, such as the German TerraSAR-X mission (2007), the Canadian RADARSAT-2 mission (2007), the Italian Cosmo-SkyMed mission (2007–2010), and the latest ESA's Sentinel-1 mission (2014), are all capable of providing services pertaining to maritime and coastal surveillance. Figure 1.2 shows ship detection results based on a high resolution RADARSAT-2 SAR image, combined with the AIS reports from the coastal network as well as data from AISSat-1. The results are collected from a trial exercise in the Malangen area, near Tromsø, in northern Norway [9, 10].

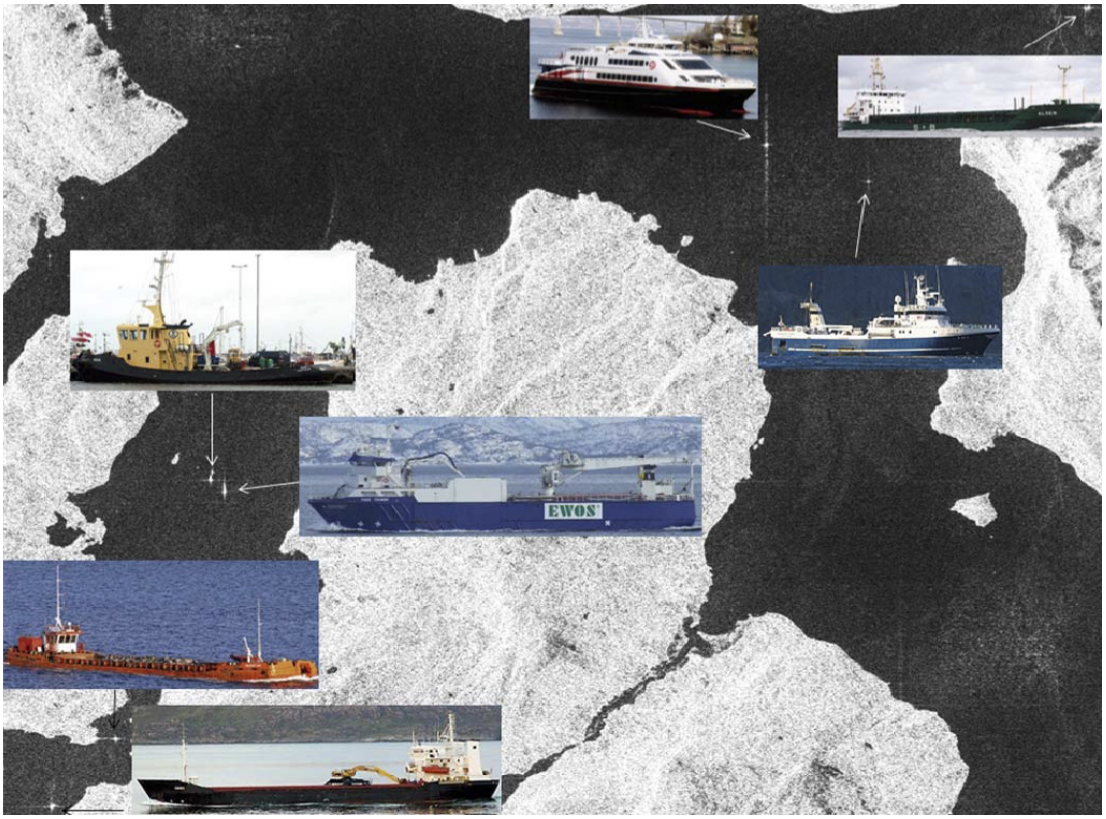

Figure 1.2: RADARSAT-2 Standard Quad-Pol SAR image in HH polarization acquired on 19^{th} September 2010. The image shows seven ships that are detected in the SAR image and confirmed by aisonline.com (from [10]).

1.3 Objectives and scope

This thesis focuses on maritime target detection using advanced SAR technology. Four research articles are included in this thesis, which provide rigorous statistical analysis of sea clutter and address challenging detection issues due to multiple targets situations and various non-homogeneous sea environments.

In order to develop robust and effective target detection algorithm for various operational maritime monitoring conditions, the specific objectives of the thesis can be summarized as:

- to explore the statistical modeling of the sea clutter in SAR images (article 1 – 4);
- to inspect the conventional target detection algorithms (article 3 – 4);
- to address the common target detection issues, i.e., capture effect and clutter edge effect (article 2 – 4);
- to develop an effective and robust target detection algorithm (article 3 – 4).

The scope of the research is aimed at vessel detection within sea clutter based on single- and multi-polarization SAR data and, therefore, certain presumptions and limitations are relevant.

Firstly, the CFAR target detection concept is adopted in the study. It usually refers to the general form of an adaptive algorithm designed to detect target signals against a varying background of noise, clutter and interference. Advanced CFAR algorithms are able to decide a detection threshold adaptively via rigorous statistical analysis of the background clutter. Meanwhile, the reference clutter is confined by a sliding window in the local background.

Both simulated and real single- and multi-polarization SAR scenes are applied in the study. The statistical characterization of the sea clutter measurements is investigated primarily on account of covariance matrix estimation for statistical modeling. Despite the popularity of choosing polarimetric methods (in the multi-polarization case), this thesis is focused on working with the intensity measurements for simplicity and practicality in real applications. Datasets are also selected to represent various real case scenarios. Note that all real SAR images are acquired in recent years covering distinct regions near or within the Norwegian Sea, the North Sea, the Portsmouth port in U.K., and offshore Netherlands. RADARSAT-2 SAR products are only considered in the study, which are provided by Norwegian Space Centre/Kongsberg Satellite Services under the Norwegian–Canadian RADARSAT agreement 2009–2013 and through Dr. A. Marino at the Institute of Environmental Engineering, ETH Zürich. Details of the individual datasets can be found in the research articles (chapter 3 to 6).

It is also worth noting that the proposed detection algorithms are equally valid for all radar sensors running at any frequency. The generality can also be extended to combining multiple data sources and handling different types of environment.

1.4 Publication summary

The main body of this thesis is presented as three journal publications and one proceedings publication, which are included as Chapters 3–6. The following summaries of the individual articles included in the thesis delineate the key concepts and highlight the main contributions of this work. Note, the papers are not presented in chronological publication order, but in an order that better indicates the research progress.

Research article I

Ding Tao, Stian N. Anfinsen, and Camilla Brekke, "**A Comparative Study of Sea Clutter Covariance Matrix Estimators**," IEEE Geoscience and Remote Sensing Letters, vol. 11, no. 5, pp. 1010–1014, May 2014.

To understand the statistics of sea clutter in multi-polarization SAR data, it is natural to study the covariance matrix derived from the scattering vector. In this letter, we

focus on the estimation of the polarimetric covariance matrix in the context of sea clutter statistical modeling. A comprehensive study of four covariance matrix estimators is provided: the maximum likelihood (ML) estimators under the Gaussian distribution (G-ML) and the K distribution (K-ML), an approximation of the latter, and a robust M-estimator. It adds to previous theoretical studies of these algorithms by evaluating their performance with respect to both estimating accuracy and computational efficiency. Experiments are performed on simulated datasets, and various texture conditions of the sea clutter are considered. In summary, the G-ML estimator is fast due to its simplicity, and it is expected to perform well under low to moderate texture conditions. The K-ML estimator models the sea clutter more accurately than the G-ML estimator under high texture but at increased computational cost. The newly proposed approximation of the K-ML estimator is comparable to the K-ML, especially with small sample sizes, while its computational cost is significantly lower than that for the K-ML estimator under all conditions. The M-estimator does not provide any distinct advantages in any of the studied cases. However, because it requires no assumption of the texture distribution, it makes an alternative to the G-ML in a highly textured clutter.

Research article II

Ding Tao, Anthony P. Doulgeris, and Camilla Brekke, "**Sea Clutter Contamination Test with Log-Cumulants**," Proc. SPIE Remote Sensing 2012, vol. 8536, no. 18, Edinburgh, United Kingdom, 24–27 Sep. 2012.

Despite the attempts of modeling the real sea clutter with more comprehensive models, non-sea-clutter targets and transitions between statistically different oceanographic conditions are always difficult to handle and likely cause inaccurate estimation of clutter properties. Referring to mixtures in the estimation window as contamination, this work introduces a novel sea clutter contamination test based on log-cumulants from Mellin kind statistics. It measures the significant deviation in log-cumulant space due to the contamination, and appears to be an effective tool for improving the sea clutter estimation or to be a direct first-stage target detector. The proposed contamination test is examined with real fine resolution quad-polarimetric RADARSAT-2 SAR measurements, from the Norwegian Sea, under various oceanographic conditions.

Research article III

Ding Tao, Stian N. Anfinsen, and Camilla Brekke, "**Robust CFAR Detector Based on Truncated Statistics in Multiple-Target Situations**," in press: IEEE Transactions on Geoscience and Remote Sensing, 2015.

In this work, a new and robust truncated statistics (TS) based CFAR (TS-CFAR) detector is proposed for vessel detection in single-look intensity and multi-look intensity

SAR images. This approach is aimed at high-target-density situations such as busy shipping lanes and crowded harbors, where the background statistics are estimated from potentially contaminated sea clutter samples. Therefore, data truncation is applied to exclude possible statistically interfering outliers and TS is exploited to model the remaining background samples. Unlike other data censoring schemes, the rigorous statistical analysis provided by TS offers improved background clutter modeling results, and does not require prior knowledge of the interfering samples. In addition, the proposed detector can be implemented with a block sliding estimation window centered at the cell under test, thus a more confined window without guard cells can be used to collect the reference samples. The comparative study has clearly demonstrated the superiority of TS-CFAR processing over conventional CFAR processors. Note that TS-CFAR detector also performs on par with iterative censoring schemes while avoiding the iterations. Overall, the TS-CFAR detection algorithm provides accurate background clutter modeling, a stable false alarm regulation property, and improved detection performance in multiple-target situations.

Research article IV

Ding Tao, Anthony P. Doulgeris, and Camilla Brekke, "**A Segmentation based CFAR Detection Algorithm using Truncated Statistics**," in review: IEEE Transactions on Geoscience and Remote Sensing, 2015.

This study looks into target detection in real non-homogeneous sea clutter environments. It is a complex and challenging task not only due to the possible capture effect from interfering outliers, but also the clutter edge effect from background intensity transitions. Based on our previous work, TS has proved to be a useful tool when the reference area is contaminated by multiple non-clutter pixels. In order to simultaneously address both issues, a robust segmentation based CFAR detection algorithm using TS is developed for multi-looked intensity SAR imagery. Within each region confined by the reference window, the proposed scheme implements an automatic image segmentation algorithm, which performs a finite mixture model estimation with a modified expectation maximization (EM) algorithm. Data truncation is applied here to exclude all possible statistically interfering classes, and the sample modeling is based upon the truncated two-parameter gamma model. Next, the CFAR detection is conducted pixel by pixel, utilizing the statistical information obtained from the segmentation process within the local reference window. The practical performance of the proposed detection algorithm is demonstrated in the experiments using real RADARSAT-2 SAR images. Compared to the conventional algorithms, the improved automatic TS based segmentation processor provides a comprehensive statistical analysis of the non-homogeneous background clutter independent from the interfering outliers. While the subsequent CFAR processor takes advantage of the available local contextual information, yields a controlled false alarm rate, and achieves excellent detection capability. Thus, our algo-

rithm is able to adapt to the complicated target situations and variations of the background clutter, and is qualified for a robust context-based fully automatic system for sea monitoring under different circumstances by SAR.

Other Publications and Presentations

As first author:

Ding Tao, Camilla Brekke, and Stian N. Anfinsen, "An Experimental Study on Ship Detection based on The Fixed-Point Polarimetric Whitening Filter," Proc. SPIE Remote Sensing 2011, vol. 8180, no. 36, Prague, Czech Republic, 19–22 Sep. 2011.

Ding Tao, Stian N. Anfinsen, and Camilla Brekke, "Ocean Clutter Modeling for Ship Detection," Proc. SEASAR 2012, Tromsø, Norway, 18–22 Jun. 2012.

Ding Tao, Stian N. Anfinsen, and Camilla Brekke, "A Ship Detection Algorithm based on Truncated Statistics," Proc. EUSAR 2014, Berlin, Germany, 2–6 Jun. 2014.

As coauthor:

Stian N. Anfinsen, Ding Tao, and Camilla Brekke, "Improved Target Detection in Polarimetric SAR Images by Use of Mellin Kind Statistics," Proc. POLinSAR 2011, Frascati, Italy, 24–28 Jan. 2011.

Dingsheng Hu, Stian N. Anfinsen, Ding Tao, and Xiaolan Qiu, "Investigation of Variations in the Equivalent Number of Looks for Polarimetric Channels," Proc. POLinSAR 2015, Frascati, Italy, 26–30 Jan. 2015.

Chapter 2

Maritime Target Detection using Synthetic Aperture Radar

This chapter first introduces the fundamentals of SAR imaging, where the basic concepts and imaging process of a polarimetric SAR (PolSAR) system are presented. Next, the statistical analysis of the SAR image is discussed with emphasis on space-borne maritime applications, including different data formats and common sea clutter modeling hypotheses. Finally, the essentials of a CFAR target detection process are summarized, followed by discussions of the primary detection issues and a short review of the known detectors.

2.1 Fundamentals of SAR imaging

Nowadays, SAR has become a well-developed radar remote sensing system, which is capable of producing high-resolution images of the Earth's surface. The SAR system is an active system, which illuminates a target's surface with microwave pulses and measures the backscattered signals to determine the characteristics of the target. Because such a system has its own illumination source, it is able to work at any time of day or night, regardless of solar illumination [16]. Additionally, SAR imaging are significantly less affected by clouds, fog, rain, snow, etc. than the visible and infrared sensors, which allows it to be an all-weather system [17].

A detailed description of SAR operations and signal processing is complex and beyond the scope of this thesis. Instead, the rest of this section is intended to provide an overview of the SAR imaging process, but more detailed information can be found in many dedicated literatures [16–27].

2.1.1 Basic concepts of polarimetric SAR

A typical radar system uses the microwave portion of the electromagnetic spectrum ranging from 3 MHz to 300 GHz in frequency, while space-borne SAR systems usu-

ally operates at wavelengths between 0.5 cm and 75 cm [26]. A list of wavelengths and frequencies of radar remote sensing bands based on IEEE standard 521-2002 [28] are included in table 2.1. In general, the choice of the system wavelength needs to be matched to the surface feature of the targeted object. Smaller features can be better distinguished by shorter wavelength (higher frequency) bands, while long wavelength bands are more suitable for large features. Therefore, different applications can be assigned to each frequency band with variable effectiveness. The bands most used by functioning space-borne SAR systems are C band (RADARSAT-2 and Sentinel-1) and X band (COSMO-SkyMed and TerraSAR-X). The applications of a C-band SAR cover a wide range of subjects, e.g., vessel, sea ice, iceberg, and ocean wave. As for X-band SARs, because of their shorter wavelengths, they are best suited for detecting and discriminating smaller objects, and have been widely used for military reconnaissance, mapping and surveillance [26].

Table 2.1: Wavelength and frequency of radar remote sensing bands based on IEEE standard 521-2002 [28].

Band	**Wavelength**	**Frequency**
HF Band	$10 - 100$ m	$30 - 3$ MHz
VHF Band	$1 - 10$ m	$300 - 30$ MHz
UHF Band	$0.3 - 1$ m	$1000 - 300$ MHz
L Band	$15 - 30$ cm	$2 - 1$ GHz
S Band	$7.5 - 15$ cm	$4 - 2$ GHz
C Band	$3.75 - 7.5$ cm	$8 - 4$ GHz
X Band	$2.5 - 3.75$ cm	$12 - 8$ GHz
Ku Band	$1.67 - 2.5$ cm	$18 - 12$ GHz
K Band	$1.11 - 1.67$ cm	$24 - 18$ GHz
Ka Band	$0.75 - 1.11$ cm	$40 - 24$ GHz

Moreover, since radar signal is essentially an electromagnetic wave, where the electric field is perpendicular to the direction of propagation, the polarization of the wave is defined as the direction of the electric field, which can be, e.g., linear horizontal (H), linear vertical (V) and circular polarized [16, 17]. The different combination of polarizations can provide different characteristics of the target being illuminated [26]. Note that, in traditional radar systems, linear H and V polarizations are commonly chosen [25], as illustrated in figure 2.1. A co-polarization (co-pol) radar system operates with the same polarization for transmitting and receiving the signal; for cross polarization (cross-pol), different polarization is used to transmit and receive the signal. A dual polarization (dual-pol) radar system operates with one polarization to transmit the signal and both polarizations simultaneously to receive the signal; and for quad polarization (quad-pol),

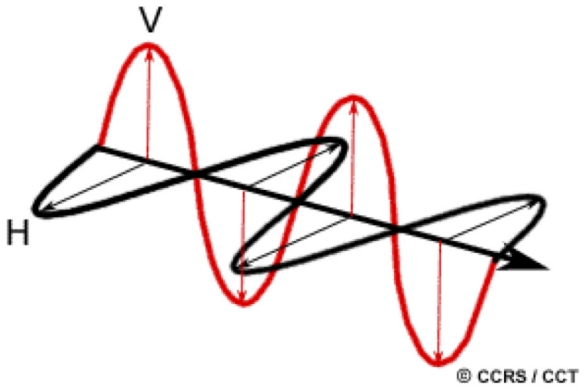

Figure 2.1: Electromagnetic waves with horizontal (H) polarization (black) and vertical (V) polarization (red). Image courtesy of Canada Centre for Remote Sensing ©CCRS/CCT [29].

H and V polarizations are used for alternate pulses to transmit the signal and with both simultaneously to receive the signal [25, 26]. As a result, multi-polarized images can be provided in the form of multiple channels (layers). Each polarization channel is identified by two letters. Thus, as many as four different channels are available, i.e., HH, HV, VH, and VV channels, where the first letter denotes the transmit polarization and the second refers to the receive polarization.

Note that, in this thesis, RADARSAT-2 single- and multi-polarization SAR products in all four possible channels are considered and applied for target detection proposes in the research articles.

2.1.2 SAR image formation

Space-borne SAR systems are capable of producing two-dimensional (2D) images. In the process, as shown in figure 2.2, a satellite-based SAR sensor moves along a flight path, the illuminated area (so called footprint) is moved along the Earth's surface in a swath (gray area), and the backscattered signals are measured and processed to construct a 2D image of the surface [16]. Compared to the naturally colored imagery derived from optical systems, each pixel in the radar image represents the radar backscatter of an area on the ground. In general, darker image areas (low backscatter) indicate that little energy of the signal is received by the radar receiver, while brighter areas (high backscatter) represent that more energy is scattered back to the radar. Also note that most current SAR systems are monostatic radar systems representing a radar having transmitter and receiver collocated in the same location, while a radar system involving separated transmitter and receiver is named bistatic radar [16].

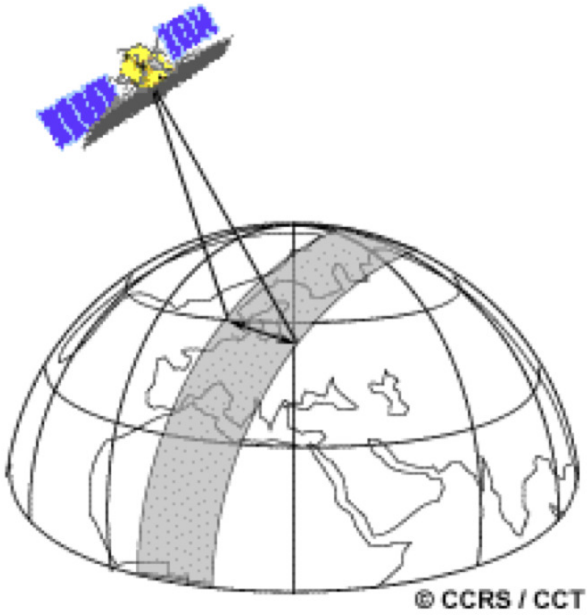

Figure 2.2: Space-borne SAR imaging. The gray area imaged on the Earth's surface, is referred to as the swath. Image courtesy of Canada Centre for Remote Sensing ©CCRS/CCT [29].

Geometric configuration

A SAR sensor needs to be mounted on a moving platform, e.g., airplane, UAV, or satellite, which operates in a side-looking geometry with an illumination perpendicular to the flight direction [29]. The typical imaging geometry is illustrated in figure 2.3. Note, an air-borne system is chosen for demonstration purpose, where the Earth's surface is assumed to be relatively flat, but the basic geometry can also be applied to space-borne systems.

As shown in the figure 2.3(a), (A) is the flight direction of the platform with the nadir (B) directly beneath the platform. The obliquely illuminated area on the ground is in the swath (S), which is usually offset from nadir. Azimuth (C) refers to the along-track dimension parallel to the flight direction, while range (D) refers to the across-track dimension perpendicular to the flight direction [29]. Figure 2.3(b) shows the illustration of the incidence angle (I), which is the angle between the radar beam and the normal to the ground surface. This angle increases from near to far range across the swath, and the return signals are normally strong at low incidence angles and decrease with increasing incidence angle. At different ranges, a slant range distance (L) is measured along the radial line of sight between the radar and each target on the ground. While the ground range distance (G) is the true distance along the ground corresponding to each point measured in slant range [29].

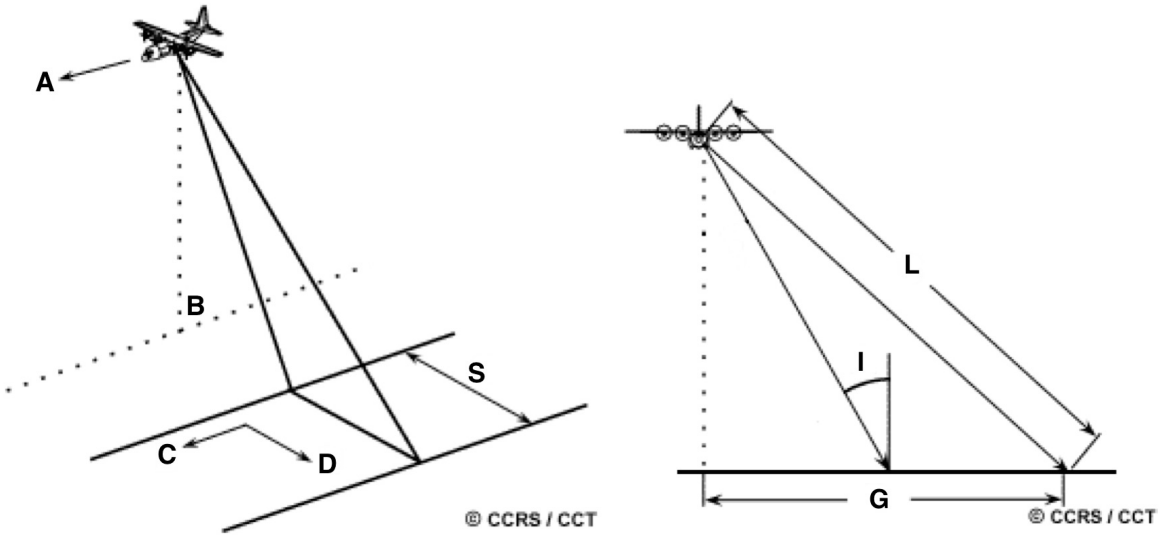

(a) (b)

Figure 2.3: Air-borne SAR imaging geometry. Image courtesy of Canada Centre for Remote Sensing ©CCRS/CCT [29].

Spatial resolution

The detail discernible in a SAR image is dependent on the spatial resolution and refers to the smallest distance between two objects that can be distinguished [25, 30]. A SAR resolution has two dimensions: the range resolution is defined by the band-width of the radar signal, and in order to achieve a higher resolution, the pulse compression technique is applied [16]; the azimuth resolution depends on the effective beam-width of the radar antenna, which is determined by built-in radar and processor constraints [16, 26]. Note that the main difference between a real aperture radar and a SAR lies in the azimuth resolution, while an aperture means the antenna opening used to collect the reflected signal. In general, the beam-width is inversely proportional to the physical size of a real antenna, for example the longer the antenna, the narrower the beam, but it is not practical for a spacecraft to carry a long antenna to achieve the desired resolution. To overcome this limitation, the SAR technique allows the system to synthesize a very long aperture by combining signals received by the radar as it moves along its flight track [16]. This principle of synthetic aperture is illustrated and explained by figure 2.4. Modern space-based commercial SAR systems, such as RADARSAT-2, COSMO-SkyMed and TerraSAR-X, orbiting at approximately seven kilometers per second, have a synthetic aperture of 17.5 kilometers. A physical antenna of that size is inconceivable.

In addition, a smaller wavelength and a shorter pulse duration can often result in a higher resolution, and the image resolution is also influenced by the incidence angle. For instance, a shallow incidence angle (at far range) can result in higher resolution,

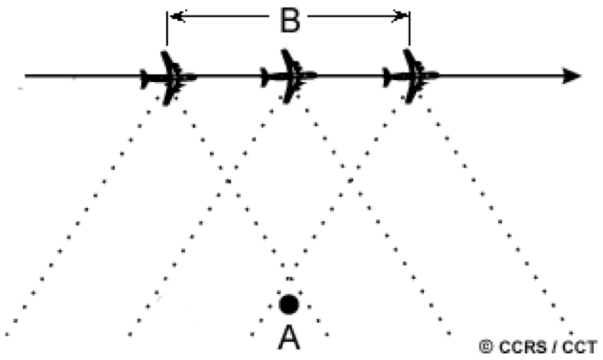

Figure 2.4: The principle of synthetic aperture. A target (A) is illuminated by a series of pulses of the radar beam. The backscattered signals from each pulse are recorded. The synthesized aperture (B) length is the distance measuring from the target enters till leaves the radar beam. Image courtesy of Canada Centre for Remote Sensing ©CCRS/CCT [29].

but the typical radar layover and shadow effects have to be considered particularly in areas with steep terrain [26]. Moreover, a SAR system operating at different acquisition modes will result in different spatial resolutions, which is discussed further in section 2.1.4.

2.1.3 Scattering mechanism

The pixel brightness in a SAR image depends on the portion of the transmitted energy that is returned back (backscattered) to the sensor from targets on the ground. The magnitude or intensity of the backscattered energy represents the interaction between the radar energy and the target surface. From the changes between the received and transmitted radar signals, various information about the scattering target can be extracted. After considering other factors like target range distance and atmospheric absorption and scattering effects, a radar scattering equation can be defined as

$$\begin{bmatrix} E_h^r \\ E_v^r \end{bmatrix} = \frac{e^{-2\pi \jmath r/\lambda}}{r} \begin{bmatrix} s_{hh} & s_{hv} \\ s_{vh} & s_{vv} \end{bmatrix} \begin{bmatrix} E_h^t \\ E_v^t \end{bmatrix} \ , \tag{2.1}$$

where r is the range distance of the target from the radar, λ is the radar signal wavelength and $\jmath = \sqrt{-1}$ is the imaginary unit. The subscript of the electromagnetic field component E_i^j, where $i \in \{h, v\}$, represents the associated polarization, and the subscript of E_i^j, where $j \in \{r, t\}$, indicates if it is transmitted or received by the radar. While s_{ab}, where $a, b \in \{h, v\}$, is the complex reflectivity (also known as the complex scattering coefficient) with the associated receive and transmit polarization, in that order. The matrix formed by the scattering coefficients is referred to as the scattering matrix $\boldsymbol{S}$. A radar image is essentially a 2D map of $\boldsymbol{S}$, which can be determined by inverting the scattering equation in (2.1).

The scattering process is primarily affected by the characteristics of the target, e.g., material properties, surface roughness, size, shape, and orientation. While the radar measurements are also influenced by target surroundings, environmental conditions, radar signal properties like wavelength and polarization, as well as the radar viewing geometry. For instance with the incidence angle, when it is small, the radar is illuminating perpendicular to the surface causing high backscatter, and when it gets larger, bigger portion of the signal is bounced away from the radar, that results in low backscatter.

Target scattering

Since the energy of the radar signal is scattered in all directions at the target's surface, the roughness of the surface largely determines the amplitude of the return signal. It is worth noting that roughness is a relative term, which needs to be considered relative to the radar signal wavelength. Illustrations of surface scatterings with moderate incidence angle under different roughness conditions are shown in figure 2.5, which generally indicate that the rougher the surface being illuminated, the brighter the backscatter (pixel) in the image. A surface is considered smooth, when its surface variations are smaller than the radar wavelength, while if the surface variations are close to the wavelength, the surface will appear rough. A smooth surface behaves like a mirror for the incident radar signal, thus most of the signal energy is reflected away according to the law of specular reflection, i.e. the reflection angle is equal to the incidence angle. For example, a flat surface of calm water normally appears as dark areas in a radar image. On the other hand, high sea states can result in moderately or very rough surface on the scale of many radar wavelengths and appear much brighter in a radar image.

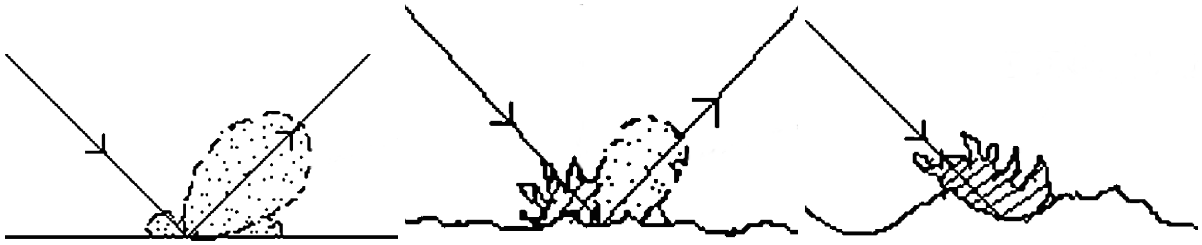

(a) Smooth surface. (b) Slightly rough surface. (c) Extremely rough surface.

Figure 2.5: Surface scatterings under different roughness conditions, i.e., smooth, slightly rough and extremely rough surfaces. Plots adapted from [31]. Image credit: Arunachalum P. Kabilan from Bannari Amman Institute of Technology and M. Paulvanna Nayaki from PSNA College of Engineering and Technology, India.

Moreover, interaction of the radar signal with a target is often more complex, due to the surroundings and the shape and size of the target. For instance, in maritime applications, different scattering situations of a vessel on the sea surface are shown in figure 2.6. A man-made vessel, as the main target in this case, is usually constructed with flat

metal surfaces, which act like a mirror reflector for most radar signals. Thus, when the surfaces are inclined towards the radar, a strong direct reflection will occur (shown in figure 2.6(a)), also known as single-bounce [16]. For most other angled surfaces, radar signals are likely to bounce between the vessel and sea surface, and then return to the radar sensor, which leads to more complicated scattering situations, as shown in figure 2.6(b) to 2.6(d).

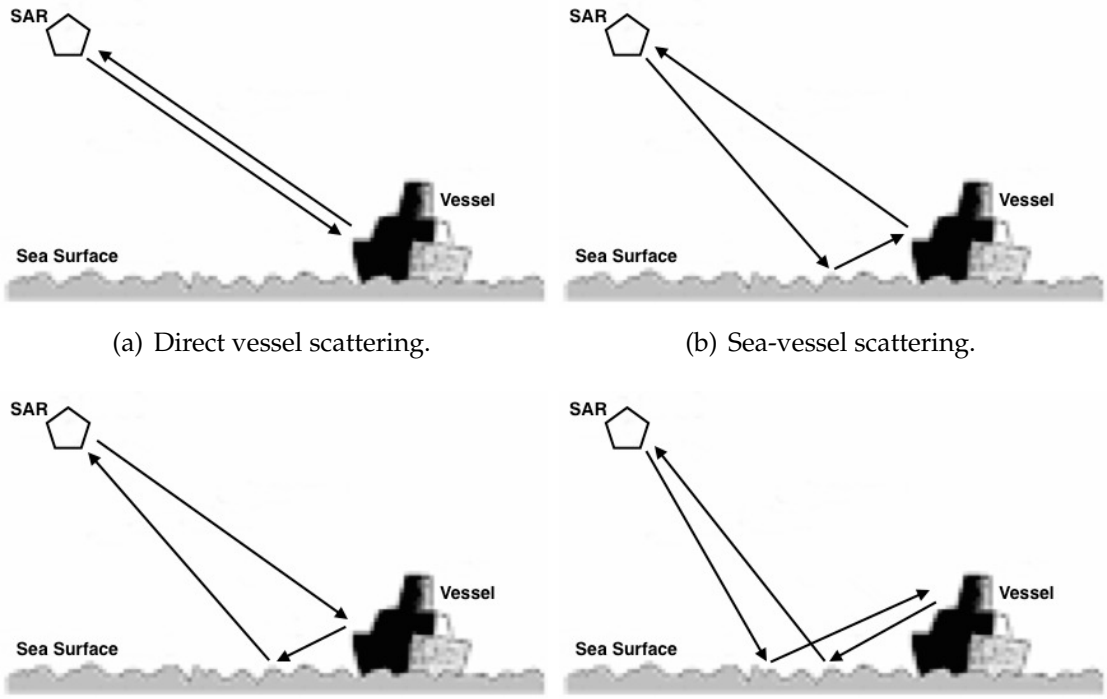

(a) Direct vessel scattering.

(b) Sea-vessel scattering.

(c) Vessel-sea scattering.

(d) Sea-vessel-sea scattering.

Figure 2.6: Different surface scattering situations for vessel over sea surface. Plots adapted from [32]. Image credit: Xu et al. from Beihang University, Beijing, China.

Note that there is a special type of reflection commonly referred to as double-bounce, which occurs when two smooth surfaces form a 90 degrees angle facing the radar signal [16]. In such case, the radar signal bounces twice off the surfaces and most of its energy is reflected back to the radar sensor. This process can be simplified and illustrated as figure 2.7. This type of reflection is very common for man-made objects, and they usually contribute to bright pixels in a radar image. For instance, vessels often have many square corners, thus the radar signal bounces directly back to the sensor. Similarly, the radar signal can bounce between the horizontal surface of the sea and the vertical surface of the vessel as shown in figure 2.6(b) and 2.6(c). Other examples with such target situations include offshore platforms, regular metallic objects like cargo containers, etc.

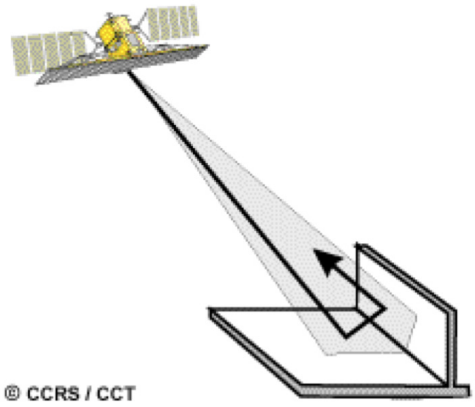

Figure 2.7: Illustration of double-bounced radar signal. Image courtesy of Canada Centre for Remote Sensing ©CCRS/CCT [29].

Speckle

Unlike optical images, SAR images are formed by the coherent interactions of the transmitted radar signal with the targets. The electromagnetic response is a measure of the integrated coherent responses from a discrete number of independent surface scatterers within the whole illuminated area. Since the number of such scatterers is unknown, the interaction process is considered random. Sea surfaces, for example, consist of a random arrangement of scattering elements, which vary from one resolution cell to another [33]. Hence, there is a noise-like phenomenon of all radar images (and of other products by similar coherent imaging systems using lasers, sonar, or ultrasound), which is known as speckle. It must be noticed that speckle has noise-like "salt and pepper" appearance, but it is not noise; it represents the real measurements of the electromagnetic returns [34]. Moreover, for a homogeneous surface with a large number of scatterers, the sum of the reflected electromagnetic waves can be assumed to have a phase uniformly distributed between $-\pi$ and π. This is often referred to as fully developed speckle [17]. A more detailed description of coherent speckle is given in [35], and the statistical model of speckle is presented in [17,23].

Speckle is traditionally suppressed by multi-look processing [36] or applying a spatial filtering on the image. In the frequency domain, the term "look" is defined as a portion of the SAR signal recorded by a part of the synthetic aperture, also known as a sub-aperture. Each sub-aperture can be processed yielding a single look image of the same scene. Thus, by averaging multiple looks incoherently, a speckle reduced multi-looked image is produced, which is known as the multi-looking processing [23,24,34]. The output image has an improved radiometric resolution, but suffers losses in geometric resolution. Frequently, multi-looking can also be achieved in the spatial domain. The simplest approach is to compute the mean power of several adjacent pixels confined by a filtering window, and this is an incoherent process as well [17]. In addition, many different filter designs have been available, such as the Frost and Lee filters [37,38] and

wavelet-based filters [39,40]. A brief review of post-processing techniques can be found in [17, 41]. Note that, in the research articles included in this thesis, both single- and multi-looked SAR images are considered for experimental and operational purposes.

2.1.4 Operational properties

Recently, many commercial SAR satellites have been or about to be put into use. Table 2.2 provides a short overview of some operating commercial SAR remote sensing missions in chronological order. More detailed information about the individual product specifications of different sensors can be found in [42–46].

Table 2.2: Commercial SAR Remote Sensing Missions.

Mission	**TerraSAR-X**	**RADARSAT-2**	**COSMO-SkyMed**	**Sentinel-1**
Launch Date	2007	2007	2007–2010	2014
Frequency Band	X	C	X	C
Acquisition Mode	**StripMap**	**Single Beam** (Standard)	**StripMap** (HIMAGE/PingPong)	**StripMap**
Polarization	single/dual	single/dual	single/dual	single/dual
Az. Resolution	3.3 m (6.6 m dual-pol.)	7.7 m	3 m (15 m dual-pol.)	5 m
Incidence Angle	15° – 60°	20° – 52°	20° – 60°	18.3° – 46.8°
Repeat Cycle	11 days	24 days	16 days	12 days

As an important operational option, the acquisition modes (highlighted in table 2.2) of a SAR sensor are directly linked with the resolution of the resulting image and the size of the scene area covered [26]. Therefore, different modes are related to the requirements of various applications. The most commonly used mode is the StripMap mode[1], in which the beam profile is kept constant throughout the imaging and data collection period. It provides a good balance between the coverage of illuminated area and the resolution. The highest resolution is offered by the SpotLight mode, when the radar beam continuously illuminates one surface area while the satellite is moving along its flight path. Meanwhile, the ScanSAR mode usually results in low resolution, but it is able to achieve a very large coverage. Thus, it is designed to be used in operations requiring large area coverage such as monitoring applications. The standard TerraSAR-X and available RADARSAT-2 acquisition modes (or beam modes) are shown in figures 2.8 and 2.9, respectively.

[1]Single Beam modes in RADARSAT-2 system are StripMap SAR modes.

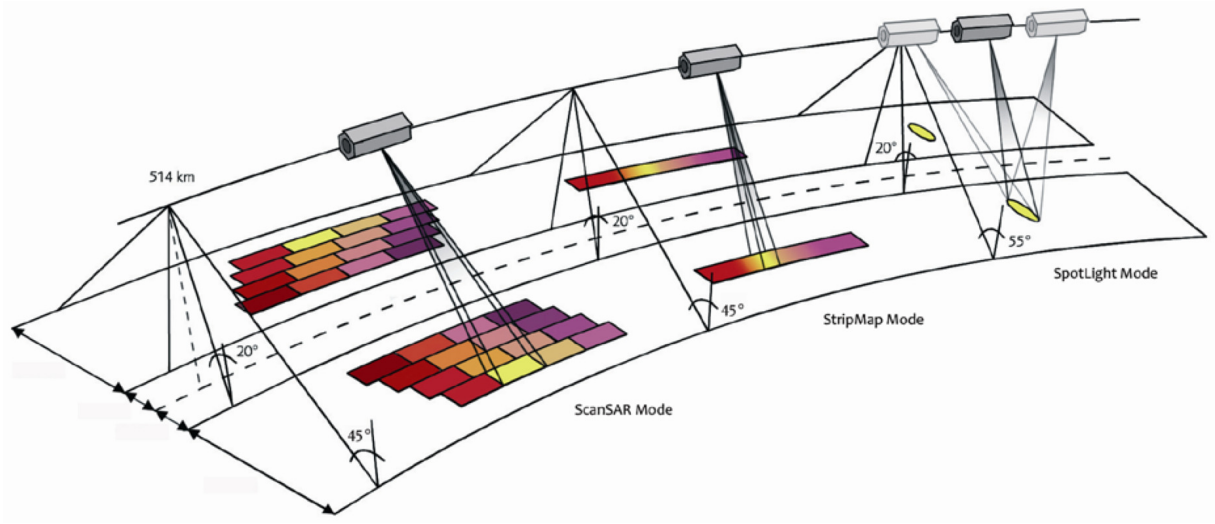

Figure 2.8: Standard TerraSAR-X acquisition modes [43]. Image courtesy of German Aerospace Center (DLR) and Airbus Defence and Space.

2.2 Statistical analysis of sea clutter

The single- and multi-polarization SAR image provides valuable information of the scattering properties of a targeted area. For numbers of maritime applications, accurate statistical analysis of sea clutter is a necessary procedure in the advanced image processing such as target detection. This section first introduces some basic concepts of the polarimetric SAR data, and provides a brief overview of the common statistical modeling approaches with emphasis on sea clutter.

2.2.1 Polarimetric SAR data

As described in previous sections, PolSAR sensors commonly use vertical-horizontal linear polarimetric basis, while other polarimetric basis can be synthesized from the two orthogonal polarizations [16, 34]. Thus a fully polarimetric SAR sensor simultaneously measures at two orthogonal polarizations and resolves all four combinations of the scattering coefficients. These four channels, HH, HV, VH and VV, are together known as the quad-pol data, which contain necessary knowledge for SAR image interpretation and analysis. Note that understanding the polarimetric basis, detailed target polarimetric characterizations and the polarimetric decomposition schemes for physical meanings are outside the focus of this thesis, and more useful information can be found in many articles such as [16, 25, 47–50].

For quad-pol data, the four complex scattering coefficients in the scattering matrix $\boldsymbol{S}$ from equation (2.1) are usually vectorized as the scattering vector, which is known as

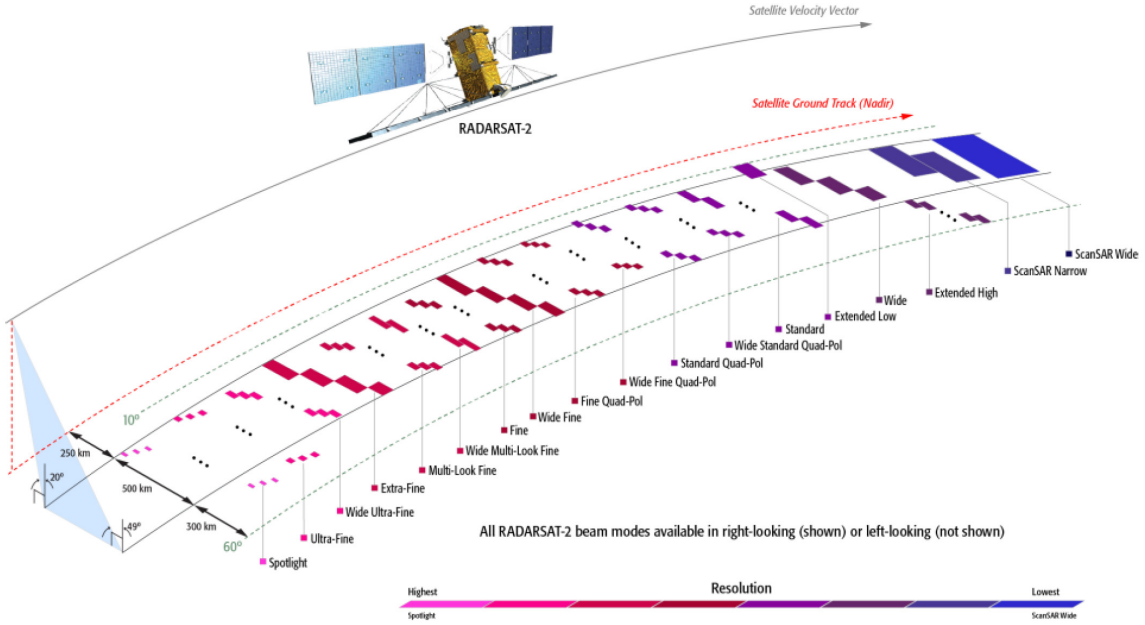

Figure 2.9: All available RADARSAT-2 acquisition modes. Image courtesy of MacDonald, Dettwiler and Associates Ltd. (MDA) ©MDA 2015.

single-look complex (SLC) data. It is defined as

$$\boldsymbol{s} = \begin{bmatrix} s_{hh} \\ s_{hv} \\ s_{vh} \\ s_{vv} \end{bmatrix}, \tag{2.2}$$

where $s_{ab} = A_{ab}e^{\jmath\theta_{ab}}$ are complex variables including both magnitude and phase information. From the complex data, many other data products can be obtained, e.g., the amplitude A, the phase θ, and the intensity $I_{ab} = |s_{ab}|^2 = A_{ab}^2$, where $|\cdot|$ refers to absolute magnitude [17]. Note that I_{ab}, where $a, b \in \{h, v\}$, is defined as the single-look intensity (SLI) for different polarimetric channels.

As an effective speckle reducing process, multi-looking has been introduced in section 2.1.3. The multi-looking operation can be formulated as

$$\boldsymbol{C} = \frac{1}{L}\sum_{i=1}^{L} \boldsymbol{s}_i \boldsymbol{s}_i^H = \begin{bmatrix} \langle|s_{hh}|^2\rangle & \langle s_{hh}s_{hv}^*\rangle & \langle s_{hh}s_{vh}^*\rangle & \langle s_{hh}s_{vv}^*\rangle \\ \langle s_{hv}s_{hh}^*\rangle & \langle|s_{hv}|^2\rangle & \langle s_{hv}s_{vh}^*\rangle & \langle s_{hv}s_{vv}^*\rangle \\ \langle s_{vh}s_{hh}^*\rangle & \langle s_{vh}s_{hv}^*\rangle & \langle|s_{vh}|^2\rangle & \langle s_{vh}s_{vv}^*\rangle \\ \langle s_{vv}s_{hh}^*\rangle & \langle s_{vv}s_{hv}^*\rangle & \langle s_{vv}s_{vh}^*\rangle & \langle|s_{vv}|^2\rangle \end{bmatrix}, \tag{2.3}$$

where L is the number of looks, the superscript ^{H} represents the Hemitian or complex transpose operator, the superscript * denotes complex conjugation, and $\langle\cdot\rangle$ refers

to ensemble averaging [17]. The output matrix $\boldsymbol{C}$ is the polarimetric covariance matrix also known as multi-look complex (MLC) data, which is positive definite and Hermitian symmetric. The diagonal elements of the covariance matrix are real-valued multilooked intensities (MLI) of different polarimetric channels, while the complex covariances are found off the diagonal. Note that $\boldsymbol{C}$ is actually the sample mean estimate of the covariance matrix. This conventional estimation has been applied as a good default option in many studies, and it is the maximum likelihood estimator only when the scattering vector $\{\boldsymbol{s}_i\}$ is assumed as complex, circular and zero mean multivariate Gaussian distributed. Since the covariance matrix estimation is considered an important factor in the statistical analysis of sea clutter in the PolSAR images, detailed studies have been conducted in the research article I (see chapter 3).

In addition, the number of looks L often needs to be replaced by the equivalent number of looks (ENL), which is a lowered version of L used pragmatically in the statistical modeling to account for correlation between the samples [51]. The ENL can be considered as an image constant and is commonly estimated from a recognized homogeneous region in a SAR image, where the speckle is fully developed and the radar cross section (RCS) is assumed to be constant [17]. The most common definition of the ENL for SAR intensity measurements is defined as [17, Ch. 4]

$$\text{ENL} = \frac{(mean)^2}{variance} \,. \tag{2.4}$$

Although, many other ENL estimators have been studied previously, e.g. [17,23,51–53], this choice is out of the scope of this thesis.

2.2.2 Sea clutter statistical modeling

In this thesis, SLI and MLI SAR images are considered in order to directly support the operational applications, where single- or dual-polarization intensity data are usually applied. A number of statistical models have been proposed and investigated previously.

In general, the product model has been widely accepted to be an appropriate statistical model for the sea clutter due to its flexibility. Based on the spherically invariant random process theory, there are two unrelated processes combined to explain the SAR image characteristics, i.e., a fully developed speckle and an underlying RCS referred to as texture [17, 54]. In the simplest form, the SAR intensity measurements I can be expressed as

$$I = \tau X \,, \tag{2.5}$$

where the real and positive random variable, $\tau \in \mathbb{R}^+$, represents the underlying texture component, and X is the uncorrelated speckle contribution. The $\mathcal{K}$ distribution [33], defined as the product of a gamma distributed texture and a Gaussian distributed speckle, has been primarily studied in this thesis for high resolution SAR sea clutter data. While

the recent $\mathcal{G}^0$ distribution [55] and $\mathcal{U}$ distribution [56] can be derived from the product model as well.

Note that when a gamma distributed texture variable is assumed, it introduces an additional shape parameter, α, indicating the texture condition; the larger (smaller) the shape parameter, the lower (higher) the texture variation level. In practice, a limited number of clutter samples are used for parameter estimation, which often leads to large variances and inaccurate results [57]. The popular moment-based methods for the shape parameter estimation have been studied extensively in previous papers [17, 58–60], and are mainly applied in the studies for their simplicities. The mth-order moment of the $\mathcal{K}$-distributed L-looked intensities is derived as

$$E\{I^m\} = E\{I\}^m \frac{\Gamma(L+m)}{L^m\Gamma(L)} \frac{\Gamma(\alpha+m)}{\alpha^m\Gamma(\alpha)} \,, \tag{2.6}$$

where $E\{\cdot\}$ is the expectation operator and $\Gamma(\cdot)$ is the gamma function. It is worth noting that, parameter estimations can also be achieved by the method of log-cumulants [34, 57], and the corresponding estimators prove superior bias and variance properties to linear moments [60–63]. This method is derived from the Mellin kind statistics [34], which relies on a logarithmic transformation of the data, thus it can be naturally applied in the statistical analysis of the product model.

For many maritime applications, non-homogenous sea clutter is commonly encountered and must be addressed. Often associated with complex target and oceanographic conditions, mixtures in the estimation window (acting as contaminations) could cause significant changes in the clutter modeling. As demonstrated in the research article II (see chapter 4), a log-cumulants based test has been developed to identify such contaminated areas, and the log-cumulants diagrams were utilized as a visualization tool to show the effects intuitively. Moreover, even though the statistical models have become increasingly comprehensive over time, there is probably still no single model to suit all situations. Therefore, a finite mixture modeling approach based on a modified EM algorithm [64, 65] was discussed and applied in this thesis. It allows a relatively simple two-parameter gamma distribution to be used in the process, and appears to be suitable for the majority of the images that were available at the time. It is also believed that many of the techniques and experience gained in the simple case will remain appropriate for the extended case. More detailed descriptions and discussions are presented in the research article IV (see chapter 6).

2.3 Maritime constant false alarm rate target detection

Based on the statistical characteristics of the sea clutter, CFAR target detection can be implemented to SAR images. This section introduces the basic concepts of the CFAR detection algorithm, followed by brief reviews of the most challenging maritime detection issues and various commonly used CFAR detection schemes.

2.3.1 Basic concepts of CFAR detection algorithm

The CFAR detection algorithm utilizes a model-based thresholding technique, in which detection thresholds are adaptively calculated based on the estimated statistical information of a local background [66–68]. A CFAR detector is often implemented with the sliding window technique on a pixel-wise basis. For each pixel or cell under test (CUT), the parameters of a hypothesized model are estimated within a confined local reference window.

In practice, a desired false alarm rate P_{FA} is first specified as the acceptable probability limit to incorrectly label a background pixel as target. It is usually set according to, e.g., the image resolution and the needs of different end applications. For instance, when running a monitoring operation covering vast sea area, the spatial resolution of SAR image is often sacrificed and users generally intend to detect all potential targets. Thus, the P_{FA} can be set to a relatively larger value. On the other hand, for high-resolution surveillance in areas with densely populated targets, e.g., harbor and channel, lower P_{FA} is often required for distinct target information extraction.

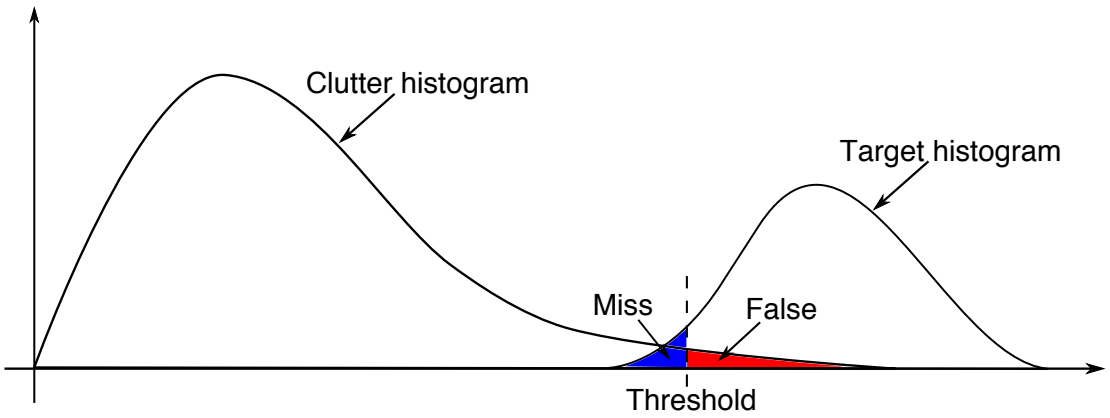

Figure 2.10: CFAR detection illustration. Blue and red areas represent detection misses and false alarms, respectively.

Figure 2.10 shows the illustration of the basic concepts of CFAR detection. As an example, an region of interest (ROI) within a SAR image is assumed and its histogram is illustrated in the figure. Note that the relative sizes of the clutter and target histograms are exaggerated for demonstration purposes, which may not indicate any real case scenario. Based on the statistical modeling of the background clutter and P_{FA}, the detection threshold is obtained, which determines the missed targets and the falsely detected clutter (false alarms). Because of the randomness of the sea clutter, the uncertainty of hypothesized model and deviation of parameter estimation, the observed number of false alarms often differs from the expected (specified) value. The observed false alarm rate is defined as

$$P_{fa} = \frac{n_{fa}}{n} \,, \tag{2.7}$$

where n_{fa} and n are the number of observed false alarms and the total number of samples within the ROI, respectively. In general, the compliance of the specified and observed false alarm rates is an indicator of the sea clutter modeling accuracy. While, a constant P_{fa} can be approached, when the statistical modeling is able to closely reflect the real measurements. This is a fundamental property, known as the false alarm regulation property, which justifies the CFAR label. In practice, the P_{FA} can commonly be set to less than 0.001% (10^{-5}) for modern fine resolution SAR images.

The performance of a CFAR detector is traditionally characterized by a plot of the detection rate versus the false alarm rate. This curve is referred to as a receiver operating characteristic (ROC), and the detection rate is measured as

$$P_d = \frac{n_d}{n_t} \,, \tag{2.8}$$

where n_d and n_t are the number of correctly detected targets and the total number of target samples, respectively. Note that the value of P_d increases monotonically with P_{FA}, which implies the trade-off between P_d and P_{FA} for a given CFAR detector. In the research article III (see chapter 5), P_d has also been examined against P_{fa} instead of P_{FA}. This makes sense when the false alarm regulation property is not satisfied, since P_{fa} represents actual performance while P_{FA} is merely a design parameter.

More relevant references of CFAR processing in radar systems can be found in [69–72].

2.3.2 Detection issues and schemes review

Detection issues

An advanced robust target detector must be able to operate under various real complex sea conditions. In general, there are two most challenging issues for non-homogeneous environments that are frequently encountered in many operational maritime applications [68,73,74].

The first one is known as the *capture effect* [75–78], which is caused by the appearance of unidentified interfering targets or other contamination sources within the local reference sea clutter [79]. The consequences usually include deceptive statistical modeling, dropping false alarm rate below the specified value, raising the detection threshold, and increasing risk of missing targets. This effect often occurs in multiple-target situations, such as busy shipping lanes, offshore oil/gas production sites and crowded harbors. The second one is recognized as the *clutter edge effect* [68,73,80], which is directly related to the background intensity transitions due to meteorological and oceanographic phenomena. There are various sea surface features resulting in such effect, e.g., transitions between regions with different wind conditions, low wind spiral marks, backscattering variations due to bathymetry, ship wake presences, etc. Since the location of the edge is unknown a priori, this issue causes great difficulties for the statistical modeling attempts based on single hypothesized model. It can also lead to an excessive number

of false alarms or a lower probability of detection around the edge area, depending on whether the CUT lies in the high or low intensity region [68]. As an example, a common maritime target detection situation is demonstrated in figure 2.11. Note that multiple bright pixels appear in the region, which indicate man-made vessels in this particular case, and there is a clear boundary (clutter edge) separating the left and right side of the image due to an incoming weather front.

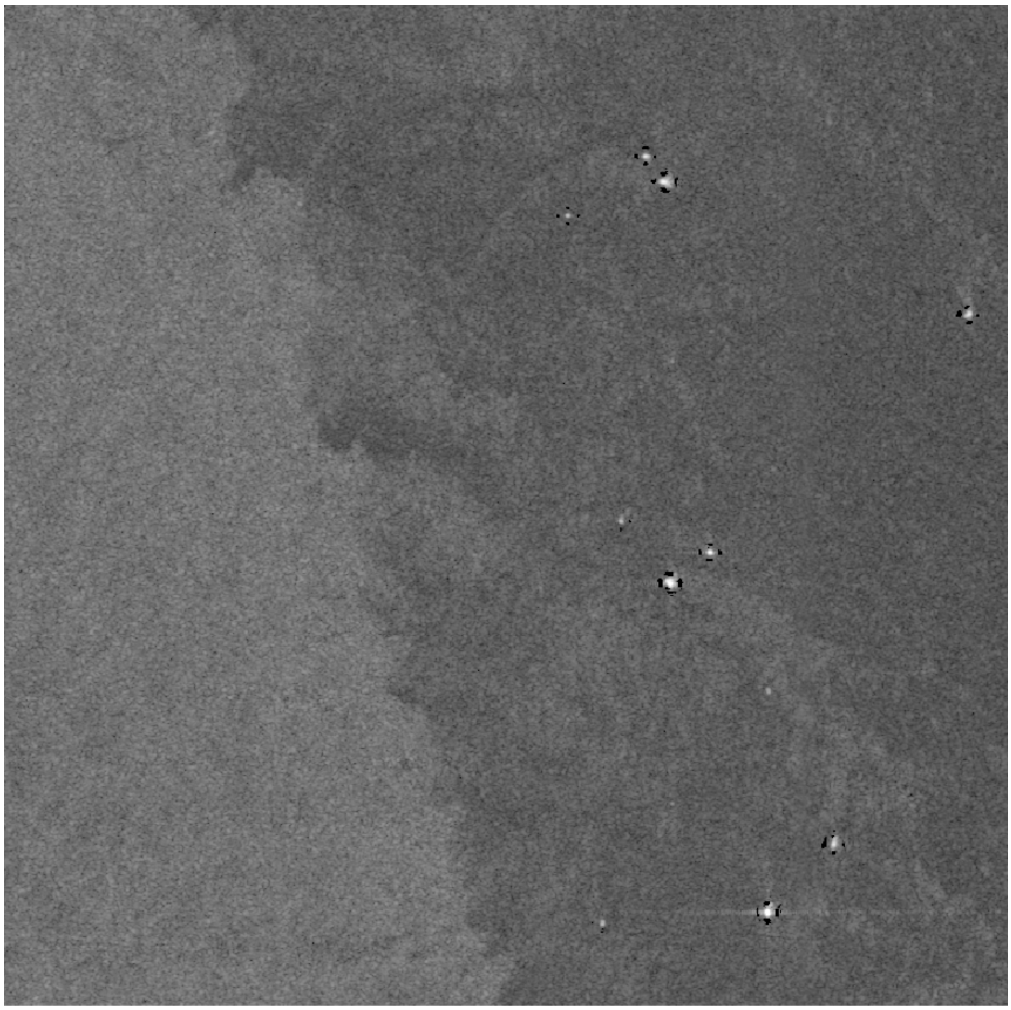

Figure 2.11: Sub-scene of a multi-looked HH polarization RADARSAT-2 SAR intensity image, acquired on 8^{th} August 2013, from the North Sea. RADARSAT-2 Data and Products ©MDA 2013 – All Rights Reserved.

Detection schemes

In history, the simplest approach to the detection of targets in SAR images is by using the traditional cell-averaging CFAR (CA-CFAR) detector [81], which represents the

background clutter by an average over the reference window. Because of its simplified assumption of a homogeneous clutter environment, a number of variations and necessary modifications have been proposed. In summary, there have been three improved schemes: the spatial sub-setting scheme, the radiometric sub-setting scheme, and the iterative censoring (IC) scheme.

The spatial sub-setting scheme divides the reference window in spatial subsets or dynamically selects a particular group of reference pixels before averaging, which includes the greatest-of CFAR (GO-CFAR) detector [82], the smallest-of CFAR (SO-CFAR) detector [83], the variability index CFAR (VI-CFAR) detector [68], etc. Such relatively simple detectors could suffer performance losses in homogeneous clutter, and are not good at handling heterogeneous clutter with complex distributions. While the ordered statistic CFAR (OS-CFAR) detector [84], as a representative of the radiometric sub-setting scheme, rank-orders the reference measurements and estimates the parameters of the hypothesized model based on the single value selected from the ordered sequence. This order statistic is more robust to outliers in multiple target situations, but losses information for estimation purposes [85]. Also as a generalization of the OS-CFAR detector, the trimmed mean CFAR (TM-CFAR) detector [86] uses the mean of a set of rank-ordered values instead. Unfortunately, its optimal performance relies on a judicious choice of the trimming parameters after prior assessment of the interfering environment [66, 74, 87]. Note that the IC scheme proposed by Barboy et al. [88] takes a different approach, in which samples that exceed an adaptive threshold are excluded from the reference clutter. The threshold is iteratively updated based on the censored reference until there are no change in the threshold and the reference clutter, thus the detection result has converged. Although the multistep adaptive procedure requires many cycles and longer calculation time, the IC scheme has shown some robust performances in recent studies [89, 90], particularly for multiple target situations. In this thesis, it has also been integrated with other CFAR detectors, such as the ICCA-CFAR and ICOS-CFAR detectors presented in the research article III (see chapter 5). In addition, there are many more hybrid CFAR detectors have been developed, such as the censored mean-level detector (CMLD) [91, 92], the generalized CMLD (GCMLD) [77], the generalized two-level CMLD (GTL-CMLD) [78], the adaptive censored greatest-of CFAR (ACGO-CFAR) detector [87], the hybrid clutter-map/L-filtering technique [93], and the automatic censored cell-averaging (ACCA) CFAR detector based on ordered data variability (ODV) [94]. It's worth noting that most hybrid schemes include its own modified data censoring procedure. However, like the IC scheme, the censoring process inevitably excludes the naturally occurring bright pixels in the sea clutter, and the remaining reference sea clutter is not always modeled in a statistically rigorous manner. As a result, there may be severe degradations of the CFAR detection performance, and this leads to the indispensable study of the truncated statistics (TS) in this thesis. More in-depth discussions can be found in the research article III and IV (see chapter 5 and 6).

Apart from the above-mentioned attempts, the region-growing technique [95] has shown some practical prospects, which is able to adaptively optimize the reference re-

gion and maintain the CFAR properties, but with an increasing computational cost. Meanwhile, in order to better manage the complex clutter conditions, an adaptive sample/region selection stage has also been inserted into the recent algorithms [96, 97]. In fact, both resulting two-stage detection schemes are naturally leading towards a general segmentation stage, which obtains the contextual information for the subsequent CFAR detection. This claim actually agrees with the main founding from other preliminary studies [80, 98]. Therefore, the final target detection algorithm in this thesis is not only supported by a rigorous statistical analysis using TS, but also makes use of an advanced EM segmentation stage.

Chapter 3

Research Article I:
A Comparative Study of Sea Clutter Covariance Matrix Estimators

Ding Tao, Stian N. Anfinsen, and Camilla Brekke

Published in: IEEE Geoscience and Remote Sensing Letters, vol. 11, no. 5, pp. 1010–1014, May 2014.

Chapter 4

Research Article II:
Sea Clutter Contamination Test with Log-Cumulants

Ding Tao, Anthony P. Doulgeris, and Camilla Brekke

Published in: Proc. SPIE Remote Sensing 2012, vol. 8536, no. 18, Edinburgh, United Kingdom, 24–27 September 2012.

Chapter 5

Research Article III:
Robust CFAR Detector Based on Truncated Statistics in Multiple-Target Situations

Ding Tao, Stian N. Anfinsen, and Camilla Brekke

In press: IEEE Transactions on Geoscience and Remote Sensing, 2015.

Chapter 6

Research Article IV:
A Segmentation based CFAR Detection Algorithm using Truncated Statistics

Ding Tao, Anthony P. Doulgeris, and Camilla Brekke

In review: IEEE Transactions on Geoscience and Remote Sensing, 2015.

Chapter 7

Conclusions and Future Perspectives

This chapter gives concluding remarks and outlines the perspectives of future research.

7.1 Concluding remarks

A new CFAR target detection algorithm has been developed for operational maritime applications based on widely-employed SAR modes, in which a modified segmentation stage using truncated statistics is adopted in order to simultaneously solve the most challenging detection issues; the capture effect and the clutter edge effect. In the study, the robust and effective performance of the algorithm has been demonstrated on various real SAR images, in difficult target situations and under complex sea surface conditions.

For the purpose of supporting operational surveillance and monitoring systems, single- and multi-polarization SAR images have been chosen due to the high-quality 24-hour all-weather coverage of space-borne radar systems. The first step of the study was to better understand the dataset, through investigations of the polarimetric covariance matrix and its estimation. In the research article I (chapter 3), a comprehensive comparative study of four covariance matrix estimators was conducted with emphasis on the sea clutter. The proposed approximation of the $\mathcal{K}$ distribution based maximum likelihood estimator has shown comparable performance to the conventional one, and the balance between the estimation accuracy and the computational efficiency was discussed as well. It is worth noting that a possible confusion was cleared regarding the usefulness of the recently promoted M-estimator, or the so-called fixed-point estimator in many previous studies. The experimental results revealed that it does not provide any distinct advantages in any of the examined cases, and may only be an alternative to the simple Gaussian distribution based maximum likelihood estimator under highly textured sea clutter conditions.

Next, in most advanced maritime detection algorithms, the statistical analysis of the sea clutter is one of the essential procedures, especially for various non-homogeneous environments. Developed for the popular product models, a novel log-cumulants based test was performed in research article II (chapter 4). It has been used to demonstrate the

influences of inaccurate statistical modeling caused by outliers and/or mixtures (defined as contaminations) within the reference clutter. Such a test has the potential to be an effective tool for improving the sea clutter estimation or a direct first-stage target detector. In addition, an associated survey on the statistical variations of sea clutter has also been done during the study, which is based on a number of sub-scenes from different real SAR images. Although the reference area size certainly plays a significant role in the analysis, the results indicate that a highly textured clutter may be mainly caused by contaminations and there is probably no single model to be flexible enough for all situations. Therefore, for target detection process, identifying and analyzing the heterogeneous areas is more efficient than applying an increasingly sophisticated model.

Of particular emphasis are this thesis's contributions to the ongoing development of the CFAR target detection algorithms. As a traditional detection practice, the CFAR concept has been applied for decades. Numerous target detectors have been proposed with particular focuses, and all claimed to provide improved detection results. In general, the ROC curve is the well-accepted indicator of a detector's performance, but the other principal CFAR property – false alarm regulation – has been frequently neglected. It is important to note that accurate statistical modeling of the reference clutter is the most fundamental requirement that actually ensures that the observed false alarm rate meets the user-specified value. Thus a modified ROC analysis between the detection rate and the observed false alarm rate was presented in the theoretical study of research article III (chapter 5), in order to characterize the actual performance trade-off.

Finally, the most challenging detection issues have been addressed when developing an optimal CFAR target detection algorithm. Unlike the previous target detection schemes, a robust and effective operational CFAR detector should be able to work in unknown target situations and under various non-homogeneous sea conditions. In simple words, the frequently encountered capture effect and clutter edge effect must be minimized. From the research articles III and IV (chapter 5 and 6), the truncated statistics and a modified segmentation stage were introduced to the detection algorithm, which have proved to be favorable and beneficial when working with real complicated SAR images. Considering the key concepts found in other schemes, the proposed algorithm is capable of:

- handling isolated contaminations without losing too much meaningful background information, which is not the case for the GO-CFAR, SO-CFAR and other ordered statistics based CFAR detectors;
- providing rigorous statistical analysis of truncated reference clutter compared to the algorithms involving data censoring processes;
- adapting to complex environments by using the contextual information obtained from the improved automatic TS based EM segmentation processor;
- simultaneously solving both of the common detection issues;
- delivering better detection performance but not sacrificing the CFAR properties.

The promising end product is generic and can be applied to both single- and multi-polarization SAR images and other frequencies than C-band that was studied here. However, during the study, the outstanding performance of the advanced segmenta-

tion algorithm allows us to reconsider the basic concepts of CFAR. It could be that the CFAR approach for target detection has become outdated for modern high resolution SAR data, or the coming superior segmentation processor actually provides a better solution for target detection, which only future research can answer.

7.2 Future perspectives

As part of the research works in the Norwegian Research Council Arctic Earth Observation and Surveillance Technologies (ArcticEO) project, the algorithms and technologies presented in this thesis have also been developed towards the increased applications and services in Northern and Arctic regions. For such dangerous and hazardous environments, this study has the potential to provide assistance for the rapid expansions of industrial and commercial activities in a safe and sustainable way.

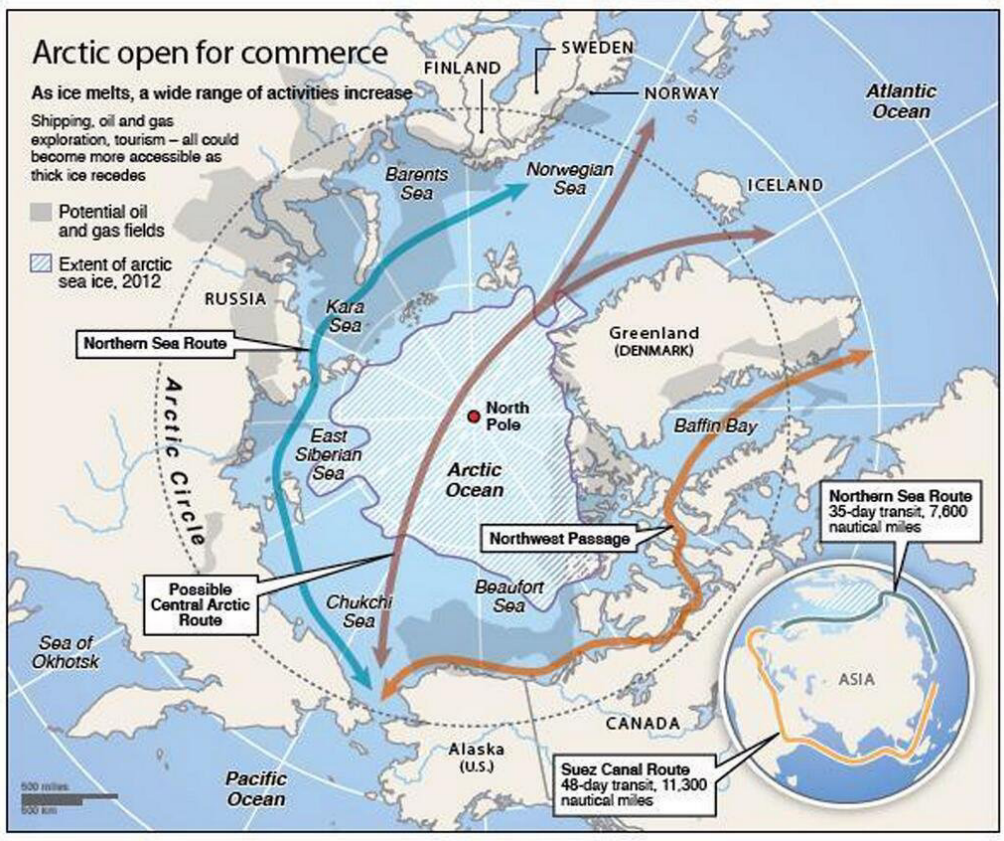

Figure 7.1: Arctic open for commerce. Image courtesy of Business Insider, from public domain www.businessinsider.com.

In the high north, the vast ice-infested waters have been experiencing dramatic changes in recent years with both positive and negative effects to human activities. As we known, due to global warming, the Arctic sea ice is shrinking in an alarmingly fast

pace. Reduced sea ice is likely to promote the maritime traffics in higher latitudes, open new shipping lanes, extend the transportation season, and provide better access to natural resources. Figure 7.1 shows the so-called polar express routes. Traditionally, there are two seasonal Arctic shipping routes connecting the Atlantic and Pacific oceans, i.e., the Northwest Passage and the Northeast Passage (also named the Northern Sea Route), which can reduce shipping times and distances significantly. Note that the possible central Arctic route could also be opened up soon. Meanwhile, a big portion of the oil and gas resources in the Arctic regions is also becoming accessible to large corporations and neighboring countries. However, the behavior and conditions of such icy waters are usually difficult to assess and predict by scientists and experts. Hazards, such as low temperatures, harsh weather, polar lows, and drifting ice objects, are obvious challenges to any functioning vessels and offshore platforms in the regions.[1]

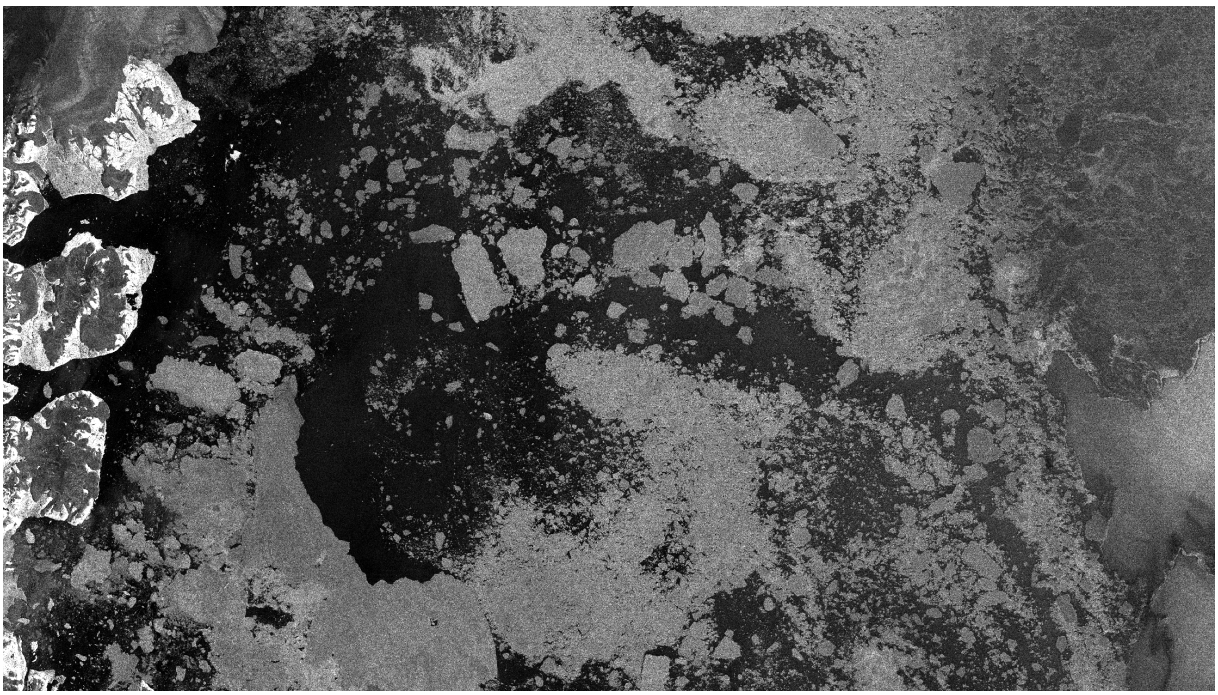

Figure 7.2: Marine environments in the Arctic. Sub-scene of a RADARSAT-2 SAR image acquired on 19^{th} August 2012, offshore Greenland. RADARSAT-2 Data and Products ©MDA 2012 – All Rights Reserved.

As an example, figure 7.2 shows a RADARSAT-2 SAR image acquired on 19^{th} August 2012, offshore Greenland, in which the multi-year sea ice breaks down to numer-

[1] According to a press release on 28^{th} September 2015 [99], the oil giant Shell announced that all drilling for oil and gas has been called off in the Chukchi and Beaufort Seas, north of Alaska, and it "will now cease further exploration activity in offshore Alaska for the foreseeable future." This announcement means that no major corporations, including Total and Statoil, is likely to drill off the Arctic coast of Alaska anytime soon, partially due to the remote and harsh environments with dangerous ice floes and frequent storms.

ous pieces floating freely during the summer. This results in a complicated marine environment and makes navigation in such region very difficult and dangerous. In addition, according to the Intergovernmental Panel on Climate Change (IPCC), the mountain glaciers worldwide are retreating at an extensive rate as well, which not only add fresh water to the sea, but also produce icebergs[1]. With only a fraction of the total volume extending above the sea surface, ice objects (ice floes, growlers and icebergs) have always been threatening and destructive to man-made objects, and are generally hard to detect by radar due to the various sizes and shapes.

Therefore, for an effective and successful ice management[2], an improved maritime monitoring and surveillance system is essential and highly requested in future Arctic developments. The proposed robust target detection algorithm is expected to have the capability of analyzing the complicated ice-infested sea clutter (as shown in figure 7.2) with the segmentation based scheme, and can be adjusted to detect densely populated floating ice objects when desired. Note that the next stage of investigations in sea ice target situations and tests in the marginal ice zones have already been on the agenda within the ArcticEO project. Moreover, many new advanced air- and space-borne SAR sensors are about to be put into use. Expected higher resolutions and extra polarimetric information exploited in the operational systems will undoubtedly lead to better detection performance and useful target discrimination ability in the next-generation target detection algorithms.

[1]Icebergs are large pieces of freshwater ice that has broken off a glacier or an ice shelf.

[2]Ice management is defined as the sum of all activities in which the objective is to reduce or avoid actions from any kind of ice features [100].

Bibliography

[1] United Nations Atlas of the Oceans, "Human Settlements on the Coast," Last checked on 31 Aug. 2015. [Online]. Available: http://www.oceansatlas.org/servlet/CDSServlet?status=ND0xODc3JjY9ZW4mMzM9KiYzNz1rb3M~

[2] International Maritime Organization, "IMO and the Environment," International Maritime Organization, 4 Albert Embankment, London SE1 7SR, United Kingdom, Tech. Rep., 2011. [Online]. Available: http://www.imo.org/en/OurWork/Environment/Documents/IMO%20and%20the%20Environment%202011.pdf

[3] Bombay Chamber of Commerce and Industry, "Making Sea Transport Clean and Green Seminar on Environmental Sustainability for the Marine Industry," Last checked on 31 Aug. 2015. [Online]. Available: http://www.bombaychamber.com/upcoming-event-award?id=195

[4] Wikipedia, "Command of the sea," Last checked on 31 Aug. 2015. [Online]. Available: https://en.wikipedia.org/wiki/Command_of_the_sea

[5] A. Leonard, A. Coburn, and G. Bowman, "Organised Crime: Piracy," 2012. [Online]. Available: http://cambridgeriskframework.com/getdocument/7

[6] International Energy Agency, *World Energy Outlook 2012*. International Energy Agency, Nov. 2012. [Online]. Available: https://www.iea.org/publications/freepublications/publication/WEO2012_free.pdf

[7] S. Kluser, J. P. Richard, G. Giuliani, A. D. Bono, and P. Peduzzi, "Illegal oil discharge in European seas," *Environ. Alert Bulletin*, Feb. 2006.

[8] International Maritime Organization, "Automatic Identification Systems (AIS)," Last checked on 31 Aug. 2015. [Online]. Available: http://www.imo.org/en/OurWork/Safety/Navigation/Pages/AIS.aspx

[9] T. Eriksen, A. Skauen, B. Narheim, O. Helleren, Ø. Olsen, and R. Olsen, "Tracking ship traffic with space-based AIS: Experience gained in first months of operations," in *Waterside Security Conference (WSS), 2010 International*, Nov. 2010, pp. 1–8.

[10] T. Hannevik, Ø. Olsen, A. Skauen, and R. Olsen, "Ship detection using high resolution satellite imagery and space-based AIS," in *Waterside Security Conference (WSS), 2010 International*, Nov. 2010, pp. 1–6.

[11] F. te Hennepe, R. Rinaldo, A. Ginesi, C. Tobehn, M. Wieser, Ø. Olsen, Ø. Helleren, R. Challamel, and F. Storesund, "Space-based detection of AIS signals: Results of a feasibility study into an operational space-based ais system," in *Advanced Satellite Multimedia Systems Conference (ASMS) and 11th Signal Processing for Space Communications Workshop (SPSC), 2010 5th*, Sep. 2010, pp. 17–24.

[12] M. A. Cervera, A. Ginesi, and K. Eckstein, "Satellite-based vessel automatic identification system: A feasibility and performance analysis," *International Journal of Satellite Communications and Networking*, vol. 29, no. 2, pp. 117–142, 2011. [Online]. Available: http://dx.doi.org/10.1002/sat.957

[13] E. Re, V. Boissinot, A. Ginesi, and C. Tobehn, "A simple high precision method for extrapolating Sat-AIS system performance," in *Advanced Satellite Multimedia Systems Conference (ASMS) and 12th Signal Processing for Space Communications Workshop (SPSC), 2012 6th*, Sep. 2012, pp. 266–272.

[14] International Maritime Organization, (1974/1980), *"International convention for the Safety of Life at Sea (SOLAS)", Chapter V "Safety of Navigation", Regulation 19*.

[15] F. Maggio, T. Rossi, E. Cianca, and M. Ruggieri, "Digital beamforming techniques applied to satellite-based AIS receiver," *Aerospace and Electronic Systems Magazine, IEEE*, vol. 29, no. 6, pp. 4–12, Jun. 2014.

[16] J.-S. Lee and E. Pottier, *Polarimetric Radar Imaging: From Basics to Applications*, ser. Optical Science and Engineering Series. Boca Raton, USA: CRC PressINC, 2009.

[17] C. Oliver and S. Quegan, *Understanding Synthetic Aperture Radar Images*, ser. SciTech radar and defense series. SciTech Publ., 2004.

[18] C. Elachi, *Spaceborne Radar Remote Sensing: Applications and Techniques*. New York: IEEE Press, 1988.

[19] J. Curlander and R. McDonough, *Synthetic Aperture Radar: Systems and Signal Processing*. New York: John Wiley & Sons, Ltd., 1991.

[20] W. Carrara, R. Goodman, and R. Majewski, *Spotlight Synthetic Aperture Radar*. Norwood, MA: Artech House, 1995.

[21] G. Franceschetti and R. Lanari, *Synthetic Aperture Radar Processing*. Boca Raton, FL: CRC Press, 1999.

[22] M. Soumekh, *Synthetic Aperture Radar Signal Processing*. New York: John Wiley & Sons, Ltd., 1999.

[23] I. G. Cumming and F. H. Wong, *Digital processing of synthetic aperture radar data : algorithms and implementation*, ser. Artech House remote sensing library. Boston: Artech House, 2005.

[24] D. Massonnet and J.-C. Souyris, *Imaging with Synthetic Aperture Radar*. Lausanne, Switzerland: EPFL Press, 2008.

[25] J. van Zyl and K. Yunjin, *Synthetic Aperture Radar Polarimetry*, ser. JPL Space Science and Technology Series. Wiley, 2011. [Online]. Available: http://books.google.co.uk/books?id=YwqkqwAR9OwC

[26] W. V. Parker, "Discover the Benefits of Radar Imaging: The Top 10 Considerations for Buying and Using Synthetic Aperture Radar Imagery," *Earth Imaging Journal*, 2012. [Online]. Available: http://eijournal.com/print/articles/discover-the-benefits-of-radar-imaging

[27] European Space Agency, "Synthetic aperture radar missions," Last checked on 31 Aug. 2015. [Online]. Available: http://www.esa.int/Our_Activities/Observing_the_Earth/Copernicus/SAR_missions

[28] IEEE, "IEEE Standard Letter Designations for Radar-Frequency Bands," *IEEE Std 521-2002 (Revision of IEEE Std 521-1984)*, 2003.

[29] Canada Centre for Remote Sensing. (2007) Fundamentals of Remote Sensing. [Online]. Available: http://www.nrcan.gc.ca/earth-sciences/geomatics/satellite-imagery-air-photos/satellite-imagery-products/educational-resources/9309

[30] C. Elachi and J. van Zyl., *Introduction to the physics and techniques of remote sensing*. Hoboken, USA: John Wiley & Sons, Ltd., 2006.

[31] A. P. Kabilan and M. P. Nayaki, "Metallic surface roughness mapping using a PC-interfaced optoelectronic sensor system," *Optical Engineering*, vol. 46, no. 10, 2007. [Online]. Available: http://dx.doi.org/10.1117/1.2799078

[32] X. Xu, Y. Wang, and Y. Qin, "SAR image modeling of ships over sea surface," in *Proc. SPIE Remote Sensing*, vol. 6363, 2006. [Online]. Available: http://dx.doi.org/10.1117/12.689788

[33] E. Jakeman and P. Pusey, "A model for non-Rayleigh sea echo," *Antennas and Propagation, IEEE Transactions on*, vol. 24, no. 6, pp. 806–814, Nov. 1976.

[34] S. N. Anfinsen, "Statistical analysis of multilook polarimetric radar images with the Mellin transform," Ph.D. dissertation, University of Tromsø, Tromsø, Norway, May 2010.

[35] J. W. Goodman, "Some fundamental properties of speckle," *Journal of the Optical Society of America*, vol. 66, no. 11, pp. 1145–1150, Nov. 1976.

[36] R. Moore, "Tradeoff between picture element dimensions and noncoherent averaging in side-looking airborne radar," *Aerospace and Electronic Systems, IEEE Transactions on*, vol. AES–15, no. 5, pp. 697–708, Sep. 1979.

[37] V. S. Frost, J. A. Stiles, K. Shanmugan, and J. Holtzman, "A model for radar images and its application to adaptive digital filtering of multiplicative noise," *Pattern Analysis and Machine Intelligence, IEEE Transactions on*, vol. PAMI–4, no. 2, pp. 157–166, Mar. 1982.

[38] J.-S. Lee, "A simple speckle smoothing algorithm for synthetic aperture radar images," *Systems, Man and Cybernetics, IEEE Transactions on*, vol. SMC–13, no. 1, pp. 85–89, Jan. 1983.

[39] M. Simard, "Extraction of information and speckle noise reduction in SAR images using the wavelet transform images using the wavelet transform," in *Geoscience and Remote Sensing Symposium Proceedings, 1998. IGARSS '98. 1998 IEEE International*, vol. 1, Jul. 1998, pp. 4–6.

[40] Z. Zeng and I. Cumming, "SAR image data compression using a tree-structured wavelet transform," *Geoscience and Remote Sensing, IEEE Transactions on*, vol. 39, no. 3, pp. 546–552, Mar. 2001.

[41] Y. Dong, A. Milne, and B. Forster, "A review of SAR speckle filters: texture restoration and preservation," in *Geoscience and Remote Sensing Symposium, 2000. Proceedings. IGARSS 2000. IEEE 2000 International*, vol. 2, 2000, pp. 633–635.

[42] German Aerospace Center (DLR), "TerraSAR-X Ground Segment Basic Product Specification Document," German Aerospace Center (DLR), Tech. Rep. TX-GS-DD-3302, Oct. 2013. [Online]. Available: http://www2.geo-airbusds.com/files/pmedia/public/r466_9_tx-gs-dd-3302_basic-product-specification-document_1_9.pdf

[43] ——, "TerraSAR-X Image Product Guide – Basic and Enhanced Radar Satellite Imagery," German Aerospace Center (DLR), Tech. Rep., Aug. 2014. [Online]. Available: http://www.geo-airbusds.com/en/228-terrasar-x-technical-documents

[44] MacDonald, Dettwiler and Associates Ltd. (MDA), "RADARSAT-2 Product Description," MacDonald, Dettwiler and Associates Ltd. (MDA), Tech. Rep. RN-SP-52-1238, May 2014. [Online]. Available: http://gs.mdacorporation.com/products/sensor/radarsat2/RS2_Product_Description.pdf

[45] Italian Space Agency (ASI), "COSMO-SkyMed SAR Products Handbook," Italian Space Agency (ASI), Tech. Rep. ASI-CSM-ENG-RS-092-A, Apr. 2007. [Online]. Available: http://www.cosmo-skymed.it/docs/ASI-CSM-ENG-RS-092-A-CSKSARProductsHandbook.pdf

[46] European Space Agency (ESA), "Sentinel-1 Product Definition," European Space Agency (ESA), Tech. Rep. S1-RS-MDA-52-7440, Jul. 2015. [Online]. Available: https://earth.esa.int/documents/247904/0/Sentinel-1+Product+Definition+V2.6/445e48a9-7f4e-4e2d-8966-e7db3ef08b8a?version=1.1

[47] S. Cloude and E. Pottier, "A review of target decomposition theorems in radar polarimetry," *Geoscience and Remote Sensing, IEEE Transactions on*, vol. 34, no. 2, pp. 498–518, Mar. 1996.

[48] R. Touzi, W. M. Boerner, J. S. Lee, and E. Lueneburg, "A review of polarimetry in the context of synthetic aperture radar: concepts and information extraction," *Canadian Journal of Remote Sensing*, vol. 30, no. 3, pp. 380–407, 2004. [Online]. Available: http://dx.doi.org/10.5589/m04-013

[49] Y. Yamaguchi, T. Moriyama, M. Ishido, and H. Yamada, "Four-component scattering model for polarimetric SAR image decomposition," *Geoscience and Remote Sensing, IEEE Transactions on*, vol. 43, no. 8, pp. 1699–1706, Aug. 2005.

[50] S. R. Cloude, *Polarisation: Applications in Remote Sensing*. Oxford, UK: Oxford University Press, 2010.

[51] S. N. Anfinsen, A. P. Doulgeris, and T. Eltoft, "Estimation of the equivalent number of looks in polarimetric synthetic aperture radar imagery," *Geoscience and Remote Sensing, IEEE Transactions on*, vol. 47, no. 11, pp. 3795–3809, Nov. 2009.

[52] J. Lee, D. Schuler, R. Lang, and K. Ranson, "K-distribution for multi-look processed polarimetric SAR imagery," in *Geoscience and Remote Sensing Symposium, 1994. IGARSS '94. Surface and Atmospheric Remote Sensing: Technologies, Data Analysis and Interpretation., International*, vol. 4, Aug. 1994, pp. 2179–2181.

[53] A. Frery, A. Correia, and C. da Freitas, "Classifying multifrequency fully polarimetric imagery with multiple sources of statistical evidence and contextual information," *Geoscience and Remote Sensing, IEEE Transactions on*, vol. 45, no. 10, pp. 3098–3109, Oct. 2007.

[54] K. Ward, "Compound representation of high resolution sea clutter," *Electronics Letters*, vol. 17, no. 16, pp. 561–563, Aug. 1981.

[55] C. C. Freitas, A. C. Frery, and A. H. Correia, "The polarimetric G distribution for SAR data analysis," *Environmetrics*, vol. 16, no. 1, pp. 13–31, 2005. [Online]. Available: http://dx.doi.org/10.1002/env.658

[56] L. Bombrun and J.-M. Beaulieu, "Fisher distribution for texture modeling of polarimetric SAR data," *Geoscience and Remote Sensing Letters, IEEE*, vol. 5, no. 3, pp. 512–516, Jul. 2008.

[57] J.-M. Nicolas, "Introduction aux statistiques de deuxième espèce: applications des logs-moments et des logs-cumulants à l'analyse des lois d'images radar," *Traitement du Signal*, vol. 19, no. 3, pp. 139–167, 2002.

[58] A. Farina, F. Gini, M. Greco, and L. Verrazzani, "High resolution sea clutter data: statistical analysis of recorded live data," *Radar, Sonar and Navigation, IEE Proceedings* -, vol. 144, no. 3, pp. 121–130, Jun. 1997.

[59] D. Iskander and A. Zoubir, "Estimation of the parameters of the K-distribution using higher order and fractional moments," *Aerospace and Electronic Systems, IEEE Transactions on*, vol. 35, no. 4, pp. 1453–1457, Oct. 1999.

[60] S. N. Anfinsen, "On the supremacy of logging," in *Proc. POLinSAR 2011*, Frascati, Italy, Jan. 2011, p. 8.

[61] S. N. Anfinsen and T. Eltoft, "Application of the matrix-variate Mellin transform to analysis of polarimetric radar images," *Geoscience and Remote Sensing, IEEE Transactions on*, vol. 49, no. 6, pp. 2281–2295, Jun. 2011.

[62] S. N. Anfinsen, A. P. Doulgeris, and T. Eltoft, "Goodness-of-Fit tests for multilook polarimetric radar data based on the Mellin transform," *Geoscience and Remote Sensing, IEEE Transactions on*, vol. 49, no. 7, pp. 2764–2781, Jul. 2011.

[63] D. Tao, C. Brekke, and S. N. Anfinsen, "An experimental study on ship detection based on the fixed-point polarimetric whitening filter," in *Proc. SPIE Remote Sensing*, vol. 8180, Prague, Czech Republic, Sep. 2011, pp. 19–22. [Online]. Available: +http://dx.doi.org/10.1117/12.898068

[64] A. P. Doulgeris, S. N. Anfinsen, and T. Eltoft, "Automated non-Gaussian clustering of polarimetric synthetic aperture radar images," *Geoscience and Remote Sensing, IEEE Transactions on*, vol. 49, no. 10, pp. 3665–3676, Oct. 2011.

[65] A. P. Doulgeris, "An automatic U-distribution and Markov random field segmentation algorithm for PolSAR images," *Geoscience and Remote Sensing, IEEE Transactions on*, vol. 53, no. 4, Apr. 2015.

[66] M. El Mashade, "Monopulse detection analysis of the trimmed mean CFAR processor in nonhomogeneous situations," *Radar, Sonar and Navigation, IEE Proceedings* -, vol. 143, no. 2, pp. 87–94, 1996.

[67] C. Alberola-Lopez, J. Casar-Corredera, and G. de Miguel-Vela, "Object CFAR detection in gamma-distributed textured-background images," *Vision, Image and Signal Processing, IEE Proceedings* -, vol. 146, no. 3, pp. 130–136, Jun. 1999.

[68] M. Smith and P. Varshney, "Intelligent CFAR processor based on data variability," *Aerospace and Electronic Systems, IEEE Transactions on*, vol. 36, no. 3, pp. 837–847, Jul. 2000.

[69] A. Farina and F. A. Studer, "A review of CFAR detection techniques in radar systems," *Microwave Journal*, vol. 29, no. 9, pp. 115–128, 1986.

[70] G. Minkler and J. Minkler, *CFAR – The Principles of Automatic Radar Detection in Clutter*. Baltimore, MD: Magellan Book Company, 1990.

[71] R. Nitzberg, *Adaptive Signal Processing for Radar*. Norwood, MA: Artech House, 1990.

[72] M. Smith, "Application of the variability index (VI) statistic to radar CFAR processing," Ph.D. dissertation, Syracuse University, Syracuse, NY, Aug. 1997.

[73] F. Soltani and M. Barkat, "CFAR binary integration detection in nonhomogeneous partially correlated clutter," *Radar, Sonar and Navigation, IEE Proceedings -*, vol. 144, no. 5, pp. 293–300, Oct. 1997.

[74] P. Tsakalides, F. Trinic, and C. Nikias, "Performance assessment of CFAR processors in pearson-distributed clutter," *Aerospace and Electronic Systems, IEEE Transactions on*, vol. 36, no. 4, pp. 1377–1386, Oct. 2000.

[75] P. McLane, P. Wittke, and C. K.-S. Ip, "Threshold control for automatic detection in radar systems," *Aerospace and Electronic Systems, IEEE Transactions on*, vol. AES-18, no. 2, pp. 242–248, Mar. 1982.

[76] E. Al-Hussaini and B. Ibrahim, "Comparison of adaptive cell-averaging detectors for multiple-target situations," *Communications, Radar and Signal Processing, IEE Proceedings F*, vol. 133, no. 3, pp. 217–223, Jun. 1986.

[77] M. Barkat, S. Himonas, and P. Varshney, "CFAR detection for multiple target situations," *Radar and Signal Processing, IEE Proceedings F*, vol. 136, no. 5, pp. 193–209, Oct. 1989.

[78] S. Himonas and M. Barkat, "Automatic censored CFAR detection for nonhomogeneous environments," *Aerospace and Electronic Systems, IEEE Transactions on*, vol. 28, no. 1, pp. 286–304, Jan. 1992.

[79] N. Balakrishnan and A. Basu, *The Exponential Distribution: Theory, Methods and Applications*. Gordon and Breach Publishers, 1995.

[80] P. Lombardo and M. Sciotti, "Segmentation-based technique for ship detection in SAR images," *Radar, Sonar and Navigation, IEE Proceedings -*, vol. 148, no. 3, pp. 147–159, Jun. 2001.

[81] H. M. Finn and R. S. Johnson, "Adaptive detection mode with threshold control as a function of spatially sampled clutter-level estimates," *RCA Review*, vol. 29, pp. 414–464, Sep. 1968.

[82] V. Hansen and J. Sawyers, "Detectability loss due to "Greatest Of" selection in a cell-averaging CFAR," *Aerospace and Electronic Systems, IEEE Transactions on*, vol. AES-16, no. 1, pp. 115–118, 1980.

[83] G. Trunk, "Range resolution of targets using automatic detectors," *Aerospace and Electronic Systems, IEEE Transactions on*, vol. AES-14, no. 5, pp. 750–755, 1978.

[84] H. Rohling, "Radar CFAR thresholding in clutter and multiple target situations," *Aerospace and Electronic Systems, IEEE Transactions on*, vol. AES-19, no. 4, pp. 608–621, 1983.

[85] S. Blake, "OS-CFAR theory for multiple targets and nonuniform clutter," *Aerospace and Electronic Systems, IEEE Transactions on*, vol. 24, no. 6, pp. 785–790, Nov. 1988.

[86] P. Gandhi and S. Kassam, "Analysis of CFAR processors in homogeneous background," *Aerospace and Electronic Systems, IEEE Transactions on*, vol. 24, no. 4, pp. 427–445, 1988.

[87] S. Himonas, "Adaptive censored greatest-of CFAR detection," *Radar and Signal Processing, IEE Proceedings F*, vol. 139, no. 3, pp. 247–255, 1992.

[88] B. Barboy, A. Lomes, and E. Perkalski, "Cell-averaging CFAR for multiple-target situations," *Communications, Radar and Signal Processing, IEE Proceedings F*, vol. 133, no. 2, pp. 176–186, Apr. 1986.

[89] G. Gao, L. Liu, L. Zhao, G. Shi, and G. Kuang, "An adaptive and fast CFAR algorithm based on automatic censoring for target detection in high-resolution SAR images," *Geoscience and Remote Sensing Letters, IEEE*, vol. 47, no. 6, pp. 1685–1697, Jun. 2009.

[90] Y. Cui, G. Zhou, J. Yang, and Y. Yamaguchi, "On the iterative censoring for target detection in SAR images," *Geoscience and Remote Sensing Letters, IEEE*, vol. 8, no. 4, pp. 641–645, Jul. 2011.

[91] J. Rickard and G. Dillard, "Adaptive detection algorithms for multiple-target situations," *Aerospace and Electronic Systems, IEEE Transactions on*, vol. AES-13, no. 4, pp. 338–343, Jul. 1977.

[92] J. Ritcey, "Performance analysis of the censored mean-level detector," *Aerospace and Electronic Systems, IEEE Transactions on*, vol. AES-22, no. 4, pp. 443–454, Jul. 1986.

[93] E. Conte, M. Lops, and A. Tulino, "Hybrid procedure for CFAR in non-Gaussian clutter," *Radar, Sonar and Navigation, IEE Proceedings -*, vol. 144, no. 6, pp. 361–369, 1997.

[94] A. Farrouki and M. Barkat, "Automatic censoring CFAR detector based on ordered data variability for nonhomogeneous environments," *Radar, Sonar and Navigation, IEE Proceedings -*, vol. 152, no. 1, pp. 43–51, Feb. 2005.

[95] E. Magraner, N. Bertaux, and P. Refregier, "Detection in gamma-distributed non-homogeneous backgrounds," *Aerospace and Electronic Systems, IEEE Transactions on*, vol. 46, no. 3, pp. 1127–1139, 2010.

[96] B. Chen, P. Varshney, and J. Michels, "Adaptive CFAR detection for clutter-edge heterogeneity using Bayesian inference," *Aerospace and Electronic Systems, IEEE Transactions on*, vol. 39, no. 4, pp. 1462–1470, Oct. 2003.

[97] A. Pourmottaghi, M. Taban, and S. Gazor, "A CFAR detector in a nonhomogenous Weibull clutter," *Aerospace and Electronic Systems, IEEE Transactions on*, vol. 48, no. 2, pp. 1747–1758, Apr. 2012.

[98] M. Sciotti and P. Lombardo, "Ship detection in SAR images: a segmentation-based approach," in *Radar Conference, 2001. Proceedings of the 2001 IEEE*, 2001, pp. 81–86.

[99] Shell News and Media Releases, "Shell updates on Alaska exploration," Last checked on 30 Sep. 2015. [Online]. Available: http://www.shell.com/global/aboutshell/media/news-and-media-releases/2015/shell-updates-on-alaska-exploration.html

[100] SFI Sustainable Arctic Marine and Coastal Technology (SAMCoT), "Ice Management and Design Philosophy," Last checked on 31 Aug. 2015. [Online]. Available: http://www.ntnu.edu/samcot/wp5